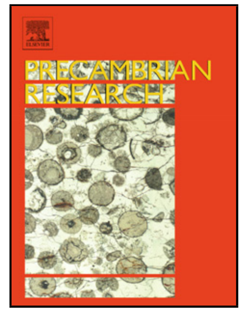

Title: Source-derived heterogeneities in the composite (charnockite-granite) ferroan Farsund intrusion (SW Norway)

Author: Jacqueline Vander Auwera Olivier Bolle Alain Dupont Christian Pin Jean-Louis Paquette Bernard Charlier Jean Clair Duchesne Nadine Mattielli Michel Bogaerts

PII:	S0301-9268(14)00194-6
DOI:	http://dx.doi.org/doi:10.1016/j.precamres.2014.06.003
Reference:	PRECAM 4007

To appear in:	*Precambrian Research*

Received date:	9-10-2013
Revised date:	3-6-2014
Accepted date:	5-6-2014

Please cite this article as: Auwera, J.V., Bolle, O., Dupont, A., Pin, C., Paquette, J.-L., Charlier, B., Duchesne, J.C., Mattielli, N., Bogaerts, M.,Source-derived heterogeneities in the composite (charnockite-granite) ferroan Farsund intrusion (SW Norway), *Precambrian Research* (2014), http://dx.doi.org/10.1016/j.precamres.2014.06.003

Source-derived heterogeneities in the composite (charnockite-granite) ferroan Farsund intrusion (SW Norway)

JACQUELINE VANDER AUWERA[a*], OLIVIER BOLLE[a], ALAIN DUPONT[a], CHRISTIAN PIN[b], JEAN-LOUIS PAQUETTE[b], BERNARD CHARLIER[a], JEAN CLAIR DUCHESNE[a], NADINE MATTIELLI[c] AND MICHEL BOGAERTS[a]

[a]*Department of Geology (B20), Université de Liège, B-4000 Liège, Belgium*

[b]*Laboratoire de Géologie, Université Blaise Pascal, 5 Rue Kessler, 63038 Clermont-Ferrand, France*

[c]*Université Libre de Bruxelles, B-1050 Bruxelles, Belgium*

* Corresponding author. Tel.:+32 4 3662253; fax: +32 4 3662029. *E-mail address*: jvdauwera@ulg.ac.be (J. Vander Auwera).

ABSTRACT

The Sveconorwegian late-orogenic magmatism of southern Norway (970-916 Ma) consists of two magmatic suites: the Hornblende-Biotite-Granitoids (HBG) suite and the Anorthosite-Mangerite-Charnockite (AMC) suite of the Rogaland Anorthosite Province (RAP), characterized by opx-bearing lithologies. The Farsund body comprises elements of both suites that display mingling relationships. The main facies, mostly charnockitic, contains orthopyroxene whereas a subordinate granitic facies comprises hornblende and biotite. U-Pb (zircon) isotopic data show overlapping ages of 931±2 Ma for the charnockitic facies and 926±4 Ma for the granitic facies. Both facies display similar extent of differentiation demonstrating that the granitic facies was not derived by fractionation from the charnockitic one. Mineralogical, geochemical and petrological data indicate that the charnockitic facies belongs to the AMC suite and the granitic facies, to the HBG suite. Strontium, Nd and Pb isotopic data show that the Farsund intrusion was emplaced at the boundary between two different lithotectonic units that are separated by the Farsund-RAP shear zone. This shear zone likely favored the emplacement of the magmas. Most of the assimilation occurred in the lower crust whereas limited differentiation likely took place in the upper crust.

Keywords: Sveconorwegian; Late-orogenic magmatism; U-Pb zircon age; Differentiation model; Sr-Nd-Pb isotopic data

1. Introduction

Granitoid rocks are essential components of the continents and despite their rather monotonous mineralogy, they have proven to be invaluable tools to decipher the structure and global differentiation of the continental crust. They were previously thought as resulting from the crystallization of large magma chambers at the level of emplacement (e.g. Buddington, 1959; Miller and Paterson, 1999), but they are now perceived by most petrologists as resulting from the addition of small batches of magmas, their composite nature being cryptic in some cases (e.g. Petford et al., 2000; Glazner et al., 2004; Vigneresse, 2004; Duchesne et al., 2013). This interpretation is supported, among others, by isotopic data which evidence significant variations in initial isotopic compositions within individual granitoids (e.g. Pressley and Brown, 1999). It has also been proposed that this assemblage of magma batches may witness the composition and heterogeneity of their lower crustal sources (e.g. Clemens et al., 2009). Another critical question is where most of the differentiation and assimilation occurs. Recent thermal modeling of the lower crust indicates that in deep crustal hot zones (Annen et al., 2006; Solano et al., 2012) it is possible to produce intermediate to silicic melts both by differentiation of mafic magma intruded as sills and/or by partial melting either of the surrounding lower crust or of previously emplaced mafic sills (the younger ones remelting the older ones). These residual and partial melts are then emplaced in the upper crust. These models suggest that an important part of assimilation and/or differentiation occurs in the lower crust.

Magmatism was abundant during the Sveconorwegian orogeny (1.1-0.93 Ga) in southern Norway, most particularly during the late-orogenic period. The Farsund body (Falkum et al., 1972; Falkum and Petersen, 1974; Falkum et al., 1979; Dupont et al., 2005; Bolle et al., 2010) is one of the southernmost late-orogenic intrusions of this orogen. In this study, we review the geology of this pluton and present new geochronological, mineral chemical, geochemical and isotopic data to show that it is made up of two different contemporaneous magmas, charnockitic and granitic, originating from different crustal sources. We infer that most of the assimilation occurred at depth in the lower crust and that magmas were rapidly transferred to their final level of emplacement without significant mixing. A limited extent of differentiation took place in the upper crust. The petrology of the Farsund intrusion was determined by its position close to both the Farsund-RAP shear zone and the opx-in isograd related to the Sveconorwegian metamorphism.

2. Geologic setting

2.1. Regional geology

The Farsund intrusion belongs to the Sveconorwegian orogen that occupies the southwestern part of the Baltic Shield and is subdivided into several segments separated by large scale N-S trending crustal discontinuities (see a recent review in Bingen et al., 2008b;

Bogdanova et al., 2008) (Fig. 1). Emplacement of widespread, late-orogenic intrusions occurred from 0.97 to 0.92 Ga (e.g. Vander Auwera et al., 2011) after the Sveconorwegian regional metamorphism that took place from 1.035 to 0.97 Ga (Bingen et al., 2008a) and grades from greenschist or epidote-amphibolite-facies in the NE to granulite facies in the SW. Two late-orogenic magmatic suites have been recognized based on petrography and geochemistry (Vander Auwera et al., 2003) (Figs. 1-2): an Anorthosite-Mangerite-Charnockite (AMC) suite (e.g. Demaiffe et al., 1986; Wilson et al., 1996; Duchesne, 2001; Bolle and Duchesne, 2007) and a suite of granitoids characterized by the abundance of hornblende and biotite (HBG suite) (e.g. Andersson et al., 1996; Andersen et al., 2001; Vander Auwera et al., 2003). The AMC suite is restricted to the westernmost and warmest part of the orogen, where it forms the Rogaland Anorthosite Province (RAP), whereas the granitoids of the HBG suite were emplaced in the rest of southern Norway. Three intrusions, including the Farsund body, identified as composite intrusions on Fig. 1 display petrographic facies corresponding to the two suites. The HBG suite is slightly older (970±6 to 932±4 Ma) than the AMC suite (932±9 to 916±9 Ma) (U-Pb on zircon: Pasteels et al., 1979; Schärer et al., 1996; Andersen et al., 2002; Bingen et al., 2006; Andersen et al., 2007; Vander Auwera et al., 2011) but the end of the the HBG magmatic event (932±4 Ma) corresponds to the beginning of the AMC suite (932±9 Ma). As synthesized by Vander Auwera et al. (2011), the AMC suite is anhydrous and contains dominant orthopyroxene together with clinopyroxene, whereas the HBG suite has a significant H_2O content (e.g. Bogaerts et al., 2006) stabilizing hornblende and biotite. Titanite is also a characteristic phase of many intrusions in the HBG suite whereas clinopyroxene is scarce and has only been observed as relic cores within amphibole (Bogaerts et al., 2003a; Bolle et al., 2003b; Vander Auwera et al., 2003). Available data also indicate that the HBG suite has a higher oxygen fugacity than the AMC suite, which translates into a higher magnetite/ilmenite ratio in the HBG suite (Vander Auwera et al.,

2011) and a pronounced positive magnetic signature on aeromagnetic surveys (Andersson et al., 1996). The HBG and AMC differentiation trends are similar, except that the AMC trend has a higher FeO_t/MgO and K_2O content and lower CaO, Sr, U, Th than the HBG trend (Vander Auwera et al., 2011). Based on radiogenic isotope data (Sr, Nd and Pb), two different crustal components, C1 and C2, have been recognized in the Sveconorwegian late-orogenic magmatism (Andersen et al., 1994; Andersen and Sundvoll, 1995; Knudsen et al., 1997; Bolle et al., 2003a; Vander Auwera et al., 2003; Vander Auwera et al., 2008). The igneous rocks with the C1 fingerprint display radiogenic initial Sr and Pb isotopes, and mildly unradiogenic initial epsilon Nd values (Sr_i = 0.735, ε_{Ndt} = -4.9). C1 was calculated as the average Sr-Nd isotopic composition of the Pre-Sveconorwegian rocks from southern Norway and was estimated from the isotopic composition of representative samples of the Pre-Sveconorwegian gneisses of the Rogaland/Vest Agder sector (Menuge, 1988; Vander Auwera et al., 2003) and of high-grade metasediments from the Bamble sector (Andersen et al., 1995; Knudsen et al., 1997). In contrast, samples with the C2 signature have lower initial Sr and Pb isotopic ratios, combined with even less radiogenic Nd (Sr_i = 0.712, ε_{Ndt} = -7.8). The C2 component corresponds to the source region of the Ubergsmoen augen gneiss unit outcropping in the Bamble sector (1.12 Ga) (Andersen et al., 1994). Andersen et al. (2001) suggested indeed that, in southern Norway, the deep continental crust has a rather uniform composition similar to the source of this unit. The C1 component has been mostly recognized in the AMC suite whereas C2 is more typical of the HBG suite. As a major crustal shear zone, the Farsund-RAP shear zone (Bolle et al., 2010), has been identified in the eastern part of the RAP and is broadly coincident with the boundary between the AMC and HBG domains (Fig. 2), it has been proposed that this steeply dipping shear zone separates two different lithotectonic units (Bolle et al., 2010; Vander Auwera et al., 2011).

Both the AMC and HBG suites display limited volumes of mafic lithologies, gabbronorites in the HBG suite, primitive opx-bearing monzodiorites (jotunites) and high-Al gabbros in the AMC suite, which display strikingly similar geochemical and radiogenic isotope (Sr, Nd, Pb) compositions (Demaiffe et al., 1990; Vander Auwera et al., 2003; Vander Auwera et al., 2008; Charlier et al., 2010; Vander Auwera et al., 2011). This observation and experimental studies performed on these rock-types (Fram and Longhi, 1992; Longhi et al., 1999) led Vander Auwera et al. (2011) to propose that they were derived by partial melting of similar lower crustal sources. These inferred lower crustal protoliths were interpreted to reflect a previous important mafic underplating having occurred in the 1.05 to 1.5 Ga period (Schiellerup et al., 2000; Vander Auwera et al., 2011). Vander Auwera et al. (2011) also emphasized the role of the subsequent Sveconorwegian regional metamorphism (from 1.035 to 0.97 Ga: Bingen and van Breemen, 1998) in modifying these underplated magmas before the start of the late-orogenic magmatism (0.97 to 0.916 Ga). Indeed, lower crustal segments were variably metamorphosed as granulite facies conditions prevailed in the westernmost part of the orogen, west of the opx-in isograd. The higher grade metamorphism produced the dehydrated lower crustal sources of the AMC suite, whereas the more hydrated sources of the HBG suite were preserved east of this isograd. The composition of the Sveconorwegian late-orogenic magmatism thus appears to have been controlled by two boundaries, the Sveconorwegian opx-in isograd and the Farsund-RAP shear zone (Fig. 2). Igneous bodies formed west of the opx-in isograd have anhydrous parageneses (orthopyroxene present), whereas those formed east of this isograd have hydrated parageneses (amphibole). West of the Farsund-RAP shear zone, the effect of the C1 isotopic component is detected in the differentiation trend, whereas east of this shear zone, the C2 signature is observed.

2.2. The Farsund intrusion

The Farsund intrusion (ca. 105 km^2: Bolle et al., 2010) is the type locality for "farsundite" (Kolderup, 1903), a term proposed as a synonym of hypersthene monzogranite but finally abandoned in the Streckeisen classification (Streckeisen, 1974) (Fig. 2). Its southern contact, partly covered by quaternary moraines, has been redefined southwards by Bolle et al. (2010) (Fig. 3). The pluton borders the Lyngdal granodiorite belonging to the HBG suite to the east and the Hidra leuconorite belonging to the AMC suite to the west. It was thus emplaced at the boundary between the AMC and HBG domains. Moreover, the Farsund intrusion is in contact with banded gneissic rocks (Falkum, 1998) that are in amphibolite facies to the NE and in granulite facies to the south (Falkum et al., 1979; Falkum, 1982, 1998). Consequently, the pluton also straddles the Sveconorwegian opx-in isograd (Fig. 2). The Farsund intrusion is separated from the Lyngdal granodiorite and the Hidra leuconorite by a thin unit of gneisses (Falkum et al., 1979; Marker et al., 2003).

Macroscopic and microscopic observations indicate that the Farsund intrusion has a dominant facies which is dark and contains orthopyroxene, and a subordinate facies significantly lighter in color and containing hornblende and biotite (Fig. 3). These two facies display a range of composition (Table 1) from intermediate (opx-bearing quartz monzonitic versus monzonitic) to silicic (charnockitic versus granitic) but will be referred to as charnockitic (Frost and Frost, 2008a) and granitic, respectively. The two facies are intermingled at various scales with frequent lobate contacts between them. Coarse- (average grain size of 2-4 mm) and fine-grained (1-2 mm) varieties have been recognized within both facies and are also locally mingled. A particularly well exposed example of mingling *within* the granitic facies is at Jøllestø, on the western coast (Fig. 3). There, a coarse-grained quartz monzonite is mingled with a finer-grained monzonite containing cm-sized plagioclase similar to those observed in the coarse grained quartz monzonite. The latter also contains lenticular enclaves of opx-bearing hornblendites several cm to several dm in size (Fig. 4A). These hornblendites essentially contain mafic minerals (hornblende, Fe-Ti oxides, apatite, zircon and orthopyroxene) and are interpreted as cumulate segregations.

The Farsund intrusion displays three other types of enclaves. The most abundant are angular enclaves, several cm to m in size, interpreted as fragments from the banded gneissic country-rocks (Fig. 4B). Less abundant leucogranitic enclaves, several dm in size, with diffuse contacts with the enclosing rock have also been observed. Rare cm- to dm- lobate microgranular enclaves (MME: Barbarin and Didier, 1992) also occur. A large body ($3km^2$) of banded gneiss has been mapped in the center of the intrusion (Fig. 3). It could correspond to a roof pendant or a pinnacle from the underlying floor (Bolle et al., 2010). Its contacts with the Farsund intrusion are not exposed. Thin (cm to dm-thickness) dikes of aplites and pegmatites have very locally been observed, mostly in the charnockitic facies.

A detailed structural study, based on the anisotropy of magnetic susceptibility (AMS) technique and combined with micro- to macrostructural observations, showed that near the contacts the Farsund intrusion is concordant with the regional structure displayed by the surrounding gneisses (Bolle et al., 2010). Minerals show microscopic textures resulting from ductile deformation: undulous extinction of quartz and feldspars, subgrains in quartz, curved polysynthetic twins in plagioclase, kinked orthopyroxene. The structural data also revealed the steeply dipping Farsund shear zone (Bolle et al., 2010) that straddles the NE border of the intrusion (Fig. 2). This shear zone has been interpreted as part of a major structure, the Farsund-RAP shear zone located east of the RAP (Bolle et al., 2010).

3. Petrography and mineral chemical composition

3.1. Petrography

As shown by Middlemost (1968), Falkum et al. (1979) and Bolle et al. (2010), amphibole, plagioclase, alkali feldspar, quartz, magnetite, ilmenite, apatite and zircon are observed in all samples whereas orthopyroxene, biotite and titanite are not ubiquitous. In the charnockitic facies, the ferromagnesian minerals are orthopyroxene and hornblende with locally some clinopyroxene and/or biotite (Fig.4 C-D). Titanite is absent and the proportion of ilmenite is generally higher than that of magnetite. Zircon and apatite occur as euhedral inclusions, mostly in orthopyroxene but also in feldspars and opaques (Fig. 4 C-D). Opaques are usually anhedral, associated with pyroxenes and locally surrounded by a thin rim of amphibole. The orthopyroxene (modal abundance of 7 to 25 %) is slightly poikilitic. It contains one or two sets of clinopyroxene exsolution (inverted pigeonite) (Fig. 4 D). Clinopyroxene also occurs as individual grains and some of these grains are clearly external granules. Plagioclase (modal abundance of 20 to 25%) is anhedral to subhedral and where locally included in K-feldspar, it displays lobated contours. K-feldspar (modal abundance of 20 to 25%) is locally a microcline, finely perthitic and contains inclusions of quartz, pyroxenes, opaques, zircon and apatite. Myrmekites at feldspar grain boundaries have been observed. Quartz (modal abundance of 10 to 25%) occurs as small rounded grains or crystals displaying irregular contours. The proportion of amphibole varies greatly and is either higher or lower than that of orthopyroxene (Fig. 3). Accordingly, some samples displaying a very low amount of orthopyroxene and locally biotite have been included in the granitic facies (see Table 1). The petrographic textures suggest early crystallization of apatite and opaques followed by orthopyroxene, plagioclase and zircon. In the granitic facies, the ferromagnesian minerals are hornblende (Fig. 4 E-F) and biotite with generally much more amphibole than biotite, titanite is abundant in many samples and the proportion of magnetite is usually higher than that of ilmenite. Petrographic textures are similar to the charnockitic facies. Amphibole (modal abundance of 20 to 30%) is mostly anhedral to subhedral locally poikilitic displaying interstitial contours toward feldspars and quartz. Apatite, opaques locally surrounded by a thin rim of titanite, zircon and amphibole form clusters. The abundance of biotite varies from none to a few grains to a few percents. It is strongly pleochroic from light brown to deep reddish brown, mostly hypidiomorphic but locally shows interstitial contacts with feldspars and quartz. It has also been observed surrounding opaques and locally partly included in amphibole. The order of crystallization is similar to the one deduced for the charnockitic facies except that the orthopyroxene is replaced by amphibole. The crystallization of biotite seems to be penecontemporaneous with or slightly later than amphibole.

The granitic facies displays no regular distribution within the intrusion as it occurs in the west and central parts as well as close to the northeastern margin (Fig. 3). It is possible that the contours of the domains occupied by the two facies of the Farsund intrusion may not have retained their magmatic aspect as they have been modified by the late subsolidus deformation (Bolle et al., 2010).

3.2. Mineral composition

Amphiboles are hastingsite except for one sample plotting in the edenite field (Fig. 5A - Supplementary Table S1A). The amphiboles from the charnockitic and granitic facies have significantly different Mg#'s (charnockitic: Mg# = 0.22-0.31; granitic: Mg# = 0.39-0.60) that partly overlap with the Mg#'s of the amphiboles from the AMC and HBG suites, respectively. Their fluorine content ranges from 0.17 a.p.f.u. up to 1.11 a.p.f.u. and increases with their Mg# (Fig. 5B). This Fe^{2+}-F avoidance, also observed in micas, has been explained by the crystal field theory, the crystal field splitting parameter being lower when Fe^{2+} is coordinated to F^- rather than to OH^- (Rosenberg and Foit, 1977).

Most low-Ca pyroxenes are ferrosilite whereas clinopyroxenes range from augite to hedenbergite (Morimoto, 1989). Heretoo, two groups of pyroxenes with low and high Mg#'s can be recognized (Fig. 5C-D, - Supplementary Table S1B-S1C) with the former overlapping in composition those of the AMC suite. In the HBG suite, clinopyroxenes (diopside) only occur as relic cores in amphiboles and have a higher Mg# than the clinopyroxenes from the Farsund intrusion.

The Fe# of biotite ranges from 0.50 to 0.76 (Fig. 5E - Supplementary Table S1D). Biotites from the Farsund samples have relatively elevated Fe# compared with biotites from the HBG suite, in agreement with what is observed for the amphiboles. Also, there is a general decrease of F/Cl versus Fe# for all samples, illustrating the same Fe^{2+}-F avoidance as in amphiboles (Rosenberg and Foit, 1977), but the trend is not well defined (Fig. 5F). Ti a.p.f.u. ranges from 0.4 to 0.6 indicating high temperatures of equilibration (Henry et al., 2005).

The composition of plagioclase (An_{24} to An_{29}) is similar to the values observed in the HBG (An_{15-31}: Vander Auwera et al., 2003) and AMC suites (An_{19-40}: Bolle and Duchesne, 2007) (Supplementary Table S1E-F). Temperatures estimated with the two-feldspar thermometer of Putirka (2008) are low (650-700°C) indicating that the feldspars re-equilibrated down to subsolidus conditions in agreement with the observed narrow range of composition and the experimental data of Bogaerts et al. (2006).

4. Whole-rock Geochemistry

Both facies recognized in the Farsund intrusion are ferroan, metaluminous and most samples straddle the boundary between the calc-alkalic and alkali-calcic fields of the MALI index (Frost et al., 2001; Frost and Frost, 2008b) (Fig. 6). The Farsund charnockite thus belongs to the group of ferroan charnockites that are frequently associated with AMCG suites (Emslie et al., 1994; Rajesh, 2007; Frost and Frost, 2008a; Rajesh, 2012). Samples overlap the fields of quartz monzonite and granite in the Ab-An-Or diagram (Fig. 7) and display high contents of Ga (Ga*10000/Al > 2.6) and incompatible elements (Zr+Nb+Ce+Y > 350 ppm) (Whalen et al., 1987) (see Table 2).

The Farsund differentiation trends display decreasing MgO, FeO_t, MnO (not shown), CaO, TiO_2, P_2O_5 and increasing K_2O with increasing SiO_2 (Fig. 8). Both facies display similar extent of differentiation (granitic facies: 59.9 to 69.4 wt wt. % SiO_2; charnockitic facies: 63.1 to 71.9wt. % SiO_2) indicating that the granitic facies was not produced by differentiation from the charnockitic one. The two facies have similar major element contents. However, the charnockitic facies has slightly higher contents of FeO and MnO that translate into higher $FeO_t/(FeO_t+MgO)$ ratios. These small differences are the same as those observed at a larger scale between the AMC and HBG suites (Fig. 8). However, the two facies have overlapping compositions in CaO and K_2O that plot between the HBG and AMC trends.

The granitic facies has higher Rb, Pb, Th and V than the charnockitic facies (Fig. 9). Again these differences are the same as those observed between the AMC and HBG suites (Fig. 9). Nevertheless, both facies have a similar Sr content that plot between the HBG and AMC trends.

The charnockitic and granitic facies have REE patterns displaying some fractionation of the LREE and a negative Eu anomaly (Fig. 10). The REE patterns of the granitic facies show slightly higher LREE fractionation and more pronounced negative Eu anomalies than the charnockitic facies (La/Yb_N = 5 to 14.5 and Eu/Eu*= 0.18 to 0.77 in the granitic facies; La/Yb_N = 3.8 to 9.7 and Eu/Eu* = 0.36 to 1.02 in the charnockitic facies). These differences are also observed between the HBG (La/Yb_N = 5.18 to 15.66; Eu/Eu* = 0.37 to 1.1) and AMC (La/Yb_N = 3.7 to 10.5; Eu/Eu* = 0.21 to 1.1) suites (Fig. 10). Several samples (AD003, AD034, AD010 in the charnockitic facies) display positive Eu anomalies (Fig. 10 and Table 2) and/or Sr and Ba contents significantly higher (98N59, AD010, MB9935 in the charnockitic facies; AD058 in the granitic facies) than the differentiation trend suggestive of some accumulation of feldspar. Sample AD058 from the granitic facies displays a lower REE content than the other samples from the same facies as it is the most differentiated one (69.36 wt.% SiO_2). The REE data presented by Petersen (1980) for a few samples of the Farsund intrusion are similar to those of the charnockitic facies (Fig. 10). .

5. Geochronology and radiogenic isotopes

Samples AD17 and AD60, selected for geochronology, are typical examples of respectively the charnockitic and granitic facies and have been collected in different areas of the intrusion (Fig. 3). No mingling was observed at the location of sample AD17 whereas mingling *within* the granitic facies, between coarse and fine-grained varieties, has been observed in the area of sample AD60. The three fractions of zircon from samples AD17 (charnockitic facies) and AD60 (granitic facies) display small degree of discordance (from negligible for AD60 up to 5% for AD17). The upper intercepts of the Concordia curve, 931±2 Ma for AD17 (charnockitic facies) and 926±4 Ma for AD60 (granitic facies) (Fig. 11, Table 3), are interpreted as crystallization ages, while the lower intercepts are considered to be geologically meaningless. These new geochronological data are in agreement with the range of 920 to 940 Ma previously proposed by Pasteels et al. (1979) based on U-Pb zircon data from sample PA70A and with geological observations (Falkum et al., 1972; Falkum et al., 1979; Bolle et al., 2010) which indicate that the Farsund intrusion is younger than the Lyngdal hornblende- and biotite-bearing granodiorite (HBG suite) dated at 950 ± 5 Ma (U-Pb zircon age; Pasteels et al., 1979). The ages of the granitic and charnockitic facies overlap within analytical errors and show that the Farsund body was emplaced at a time corresponding to the end of the HBG magmatic event (932±4 Ma) and the beginning of the AMC suite (932±9 Ma) (see review by Vander Auwera et al., 2011). The mingling relationships observed in the field between the two facies indicate their coeval character but it could be speculated that although there is a 1 Ma overlap of the analytical uncertainties at the 95% confidence level, the granitic venue, exemplified by sample AD60, corresponds to a slightly younger batch of this facies.

As can be seen in the ε_{Ndt} *vs*. $(^{87}Sr/^{86}Sr)_{930}$ (Table 4, Fig. 12A) and $(^{207}Pb/^{204}Pb)_{930}$ *vs*. $(^{206}Pb/^{204}Pb)_{930}$ (Table 5, Fig. 12B) diagrams, the granitic and charnockitic facies show significant differences. Specifically, the granitic facies has mildly negative epsilon Nd (-1 to -2) and relatively low Sr initial ratios (0.7054-0.7078) implying source materials that were both weakly enriched in LREE (moderate Sm/Nd), and in Rb relative to Sr (moderate Rb/Sr), on a time-integrated basis. In contrast, in the charnockitic facies, the initial Sr isotope signature is significantly more radiogenic, with $0.7097 < (^{87}Sr/^{86}Sr)_{930} < 0.7111$ (with one sample as high as 0.7213, possibly reflecting an inaccurate correction of ^{87}Sr ingrowth since 930 Ma), while initial epsilon Nd values scatter around zero (mean = -0.1 and SD = 0.7, for 8 data). These data imply that the *bulk* source for that group of samples was characterized by almost unfractionated LREE, combined with relatively high Rb/Sr ratios. Moreover, the $(^{207}Pb/^{204}Pb)_{930}$ and $(^{206}Pb/^{204}Pb)_{930}$ are higher in the charnockitic facies compared to values in the granitic facies. These differences in isotopic composition mimic those observed between the AMC and HBG suites (Fig. 12A-B).

6. Discussion

Mineralogy, mineral compositions, whole-rock major and trace element data as well as geochronological and isotopic data clearly indicate that the Farsund intrusion was built by the mingling of two coeval magmas, the charnockitic and granitic facies, that respectively belong to the AMC and HBG suites. This conclusion is in agreement with the emplacement of the Farsund body at the boundary between the two domains occupied by the AMC (in the west) and HBG (in the east) magmatic suites (Fig. 2) and at a time corresponding to the temporal switch from the HBG to the AMC suite. Consequently, when discussing the sources of the magmas, the differentiation processes and the crystallization conditions, we will consider two different parental magmas with reference to previous work made on the AMC and HBG suites.

6.1. Sources of the Farsund magmas

The least differentiated compositions of the granitic and charnockitic facies are, respectively, a quartz monzodiorite (sample AD60) and an opx-bearing quartz monzonite (sample AD011). In a previous study discussing the origin of the ferroan granitoids of the HBG suite and using the experimental data of Beard and Lofgren (1991) and Sisson et al. (2005) together with geochemical data, Vander Auwera et al. (2008) showed that a quartz monzodioritic composition very similar to the AD60 quartz monzodiorite could be produced either by partial melting or by fractional crystallization from a mafic (amphibolitic) composition but recognized that the partial melting process produces a better fit of the trace element data. Similarly, using experimental data acquired on opx-bearing monzodioritic (jotunitic) composition, Vander Auwera et al. (1998) showed that a an opx-bearing quartz monzonitic composition like sample AD011 could be produced by partial melting of or by fractional crystallization from an anhydrous mafic source in reducing conditions. It is also possible that both processes, fractional crystallization and partial melting, occurred simultaneously. In Farsund, no mafic (gabbroic) composition has been observed suggesting that in this case, partial melting could the dominant process. Partial melting of lower crustal sources has also been proposed by Emslie et al. (1994), Rajesh and Santosh (2004) and Rajesh (2007) as a plausible process to produce ferroan charnockitic magma.

6.2. Differentiation of the Farsund magmas

The charnockitic and granitic facies display a differentiation trend from 63.1 to 71.9 wt.% SiO_2 and from 59.9 to 69.4 wt.% SiO_2, respectively**.** A detailed discussion of the possible differentiation processes (see Supplementary material) shows that fractional crystallization was the dominant process. The same conclusion was reached for the charnockites of the nearby Bjerkreim-Sokndal layered intrusion and the Apophysis, both belonging to the AMC suite (Duchesne and Wilmart, 1997; Bolle and Duchesne, 2007).

In order to model the fractional crystallization process, the least and most differentiated samples belonging to both facies have been selected. Samples in which some accumulation of feldspar (see section 4) may have occurred, have not been considered in the modeling. In the charnockitic facies, sample AD011 (64.4 wt.% SiO_2) was considered as a plausible starting composition (L_0) and sample AD23 (69.9 wt.% SiO_2) as the residual liquid (L_1). Mineral compositions were mostly selected among the experimental phases obtained by Bogaerts et al. (2006) because sample 98N06 (64.8 wt.% SiO_2) used by these authors has a similar composition to AD011 (see Table 6) and because a larger range of mineral compositions is available in the experimental dataset thus enabling to select intermediate mineral compositions. The least square regression method indeed calculates a bulk cumulate. Subtraction of a cumulate composed of plagioclase (74.7%), orthopyroxene (4.1%), clinopyroxene (3.4%), ilmenite (4.1%), magnetite (11%) and apatite (2.6%) drives the liquid from L_0 to L_1 after 26% of crystallization with Σr^2 of 0.16 (Table 6). This calculated cumulate compares rather well with the experimental data of Bogaerts et al. (2006) on 98N06, except that it has a significantly higher proportion of plagioclase and a lower proportion of clinopyroxene than observed in the experimental charges (experimental charge 06-27: 53% plagioclase, 4% orthopyroxene, 10% clinopyroxene, 3% ilmenite, 6% magnetite, 2% apatite and 22% biotite). Since the liquidus of the plagioclase is significantly reduced when H_2O increases in the melt, we interpret the above discrepancies as resulting from a higher proportion of H_2O in the experimental charge (4.2 wt.%) compared to the Farsund magma. This induces a lower proportion of plagioclase and thus a higher proportion of clinopyroxene, the other calcic phase of the cumulate. Biotite is abundant in the experimental charge and absent in the charnockitic facies. We interpret this difference as resulting from the significantly lower Fe# (0.7) of the starting composition 98N06 used by Bogaerts et al. (2006) compared to the Fe# (0.87) of sample AD011. Indeed, the stability field of biotite decreases with increasing Fe# (Frost and Frost, 2008a). The calculated cumulate has been further tested using trace elements and the Rayleigh distillation law:

$$C_L = C_0 . F^{(D-1)}$$

where C_L and C_0 are the concentrations of the trace element in, respectively, the residual liquid and the starting compositions, F is the fraction of residual liquid that has been derived from the least square regression method and D, the bulk partition coefficient $D = \Sigma D_i.X_i$ where D_i is the partition coefficient of the trace element between the mineral i and the liquid and X_i is the fraction of the mineral i in the subtracted cumulate.

Partition coefficients were selected from the literature for dacitic to rhyolitic compositions and are listed in Table 7. Zircon, known for its high partition coefficients for HREE, was a fractionating phase as Zr decreases with increasing SiO_2 (Fig. 9). A small proportion of zircon was thus added to the subtracted cumulate. This proportion was estimated by mass balance, considering that all Zr is in the zircon and knowing the fraction of residual liquid (F=0.74). The proportion of zircon calculated in this way is 0.17%. The calculated residual liquid compares well with the observed composition thus supporting the bulk cumulate obtained from the least square regression method (see Supplementary Table S2). However, the calculated Ba content (1204 ppm) is higher than observed (977 ppm), suggesting that either the proportion of plagioclase in the cumulate, the main Ba carrier, is too low, or the partition coefficient selected for Ba is too low (1.8: Table 7). The second hypothesis appears more plausible as the calculated Sr content, another element strongly depending on the proportion of plagioclase in the cumulate, compares well with the observed one. A partition coefficient of 2.74 for Ba would produce a residual liquid with 977 ppm Ba. Such high values for D_{Ba} have been reported by several authors (Nagasawa, 1973; Nash and Crecraft, 1985; Villemant, 1988; Mahood and Stimac, 1990).

In the granitic facies, samples AD60 (59.9 wt.% SiO_2) and AD004 (65.1 wt.% SiO_2) were selected respectively for the starting composition (L_0) and the residual liquid (L_1). Subtraction of a bulk cumulate composed of plagioclase (39.1%), amphibole (46.8%), biotite (2.8%), ilmenite (1.9%), magnetite (5.4%) and apatite (3.7%) drives the liquid from L_0 to L_1 after 25% of crystallization with Σr^2 of 0.0008 (Table 6). Given the Zr contents of L_0 and L_1, the proportion of zircon in the cumulate was calculated at 0.34% by mass balance. Here, the calculated cumulate contains a proportion of plagioclase that compares very well with the experimental data obtained on sample 98N50 (59.6 wt.% SiO_2) by Bogaerts et al. (2006) at a 5.4% H_2O in the melt (experimental charge 50-31: 33% plagioclase, 52% amphibole, 5% biotite, 4% ilmenite, 4% magnetite, 2% apatite). This better fit in the case of the granitic facies is no surprise as the Lyngdal granodiorite belongs to the HBG suite and displays the granitic facies. The calculated trace elements composition of L1 (see Supplementary Table

S3) is in good agreement with the observed composition. It is worth noting that given the restricted range of SiO_2 in both facies, the fraction of liquid is high (0.75) at the end of the differentiation.

These calculations show that it is possible to predict both differentiation trends with a fractional crystallization process. In this case, disequilibrium crystallization occurs because crystals are chemically isolated from the residual liquid either by mechanical separation or because diffusion is too slow. As already mentioned, ultramafic segregations essentially made up of amphibole, pyroxene, Fe-Ti oxides, apatite and zircon with some plagioclase were observed locally, at Jøllestø (Fig. 3-4A). In the field, these segregations differ from the inclusions of banded gneisses (Fig. 4B) that are also observed in Farsund, in having a higher color index and lacking a clear schistosity. These segregations indicate that some mechanical separation, between minerals of high (ferromagnesian) and low density (plagioclase), was indeed possible in the Farsund magmas, possibly because of their rather low viscosities (see Supplementary material). Noteworthy, the calculated cumulate of the granitic trend is very similar to the measured composition of sample AD067, one of the ultramafic segregations (Table 2). These observations thus support the interpretation in terms of fractional crystallization. The Farsund major and trace elements differentiation trends are linear in Harker plots whereas in theory, fractional crystallization should produce curved trends. However, because bulk partition coefficients are mostly less than three, the power laws trajectories are rather flat and produce nearly linear trends. Also, the differentiation trends will also be affected by variations in partition coefficients resulting from evolving melt and mineral compositions. As pointed out by Clemens and Stevens (2012), « phenocrysts unmixing », a process by which a fixed crystal assemblage is progressively separated from the residual melt after some degree of crystallization took place, would also produce linear trends in variation diagrams. These are the same as those resulting from a fractional crystallization process if the separated mineral assemblage has the same mineral composition as the cumulate. This process depends on the efficiency of fractionation.

We conclude that in the Farsund magmas, the main cause of heterogeneity, and the occurrence of two facies, were inherited from the source. Mixing was inefficient (as an homogeneisation mechanism) between the two parent magmas and within each facies (see Supplementary material). Both differentiation trends can be predicted by fractional crystallization, but « phenocrysts unmixing » might also account for the data. Indeed, these processes are not mutually exclusive.

The initial Sr and Pb isotopic composition of the granitic and charnockitic facies are different whereas their Nd isotopes display a more continuous trend. As Sr and Pb are relatively more mobile than Nd, the different Sr and Pb isotopic compositions could result from the interaction with fluids (e.g. Romer et al., 2005). However, we think that this hypothesis is highly unlikely in the case of the Farsund intrusion for three reasons. First, no evidence of fluid circulation (miaroles, veins) was observed in the field and pegmatitic and aplitic dykes are very scarce. Second, the magmas were below fluid saturation (see section 6.3) thus precluding the exsolution of magmatic fluid and percolation of brines. Third, the surrounding rocks were metamorphosed mostly at granulite facies conditions before the emplacement of the intrusion.

The persistence of different isotopic compositions in the two facies shows that most of the assimilation took place before emplacement. Indeed, if their isotopic composition was controlled by assimilation of the surrounding rocks during rising and/or emplacement, they should display overlapping isotopic compositions. Moreover, their contrasted isotopic compositions correspond at a larger scale to the isotopic compositions displayed by the HBG and AMC suites, respectively. We take this as evidence that the different isotopic compositions of the two facies do not result from one being contaminated by the surrounding rocks and the other not. Following the above hypothesis on the origin of the least differentiated compositions of the Farsund intrusion, we suggest that contamination occurred in the lower crust, probably by bulk assimilation when the partial melting process took place. The opx-bearing quartz monzonitic magma, assimilated the C1 crust whereas the quartz monzodioritic magma assimilated the C2 crust. The extent of this assimilation has been estimated by Bolle et al. (2003a) and Vander Auwera et al. (2008) to about 10% but this is a tentative estimation as it strongly depends on the trace elements (Sr, Nd) content of the C1 and C2 components for which no precise constraint currently exists. The important point is that isotopic data show that the different batches of magmas that made the Farsund pluton were variably contaminated in the lower crust before their ascent in the upper crust.

6.3. P-T-fH_2O conditions of the Farsund magmas

The pressure of emplacement and crystallization has been estimated with the Al-in-hornblende geobarometer of Johnson and Rutherford (1989) as amphibole is ubiquitous even though in very low abundance in some samples of the charnockitic facies. This geobarometer was selected since crystallization took place under water-undersaturated conditions (see below). The average pressure of emplacement based on the analyses of 108 amphiboles is 410±40 MPa, with concordant results for the two facies. This result is in agreement with the pressure range of emplacement (200-400 MPa) estimated for the nearby Lyngdal granodiorite, based on experimental data on two representative samples (Bogaerts et al., 2006).

Apatite saturation temperatures overlap in both facies, 1044°C to 886°C in the charnockitic facies and 1085°C to 800°C in the granitic facies (Table 2), and indicate that apatite is a liquidus phase in agreement with the continuous decrease of P_2O_5 with increasing SiO_2 (Fig. 8). Apatite reached saturation at a slightly higher temperature in the granitic facies probably because of the higher P_2O_5 content of this facies. Zircon saturation temperatures are significantly lower, between 699°C and 941°C with an average of 849°C (Table 2) indicating that zircon was a late crystallizing phase. These high temperatures (1020°C and 900°C) agree with the experimental results (1025°C-750°C) obtained on two samples (98N50 - 59.6 wt.% SiO_2 - and 98N06 - 64.8 wt.% SiO_2) of the Lyngdal intrusion (Bogaerts et al., 2006) and more generally with estimates on igneous charnockites (Frost and Frost, 2008a).

The H_2O content in the charnockitic and granitic magmas has been estimated using the phase diagrams of Bogaerts et al. (2006). As mentioned above, sample 98N06 (Lyngdal granodiorite) is similar to AD011 (charnockitic facies) except that it has a lower Fe# (0.7) than the latter (0.87). Sample 98N50 (Lyngdal granodiorite) is close to AD60 (granitic facies) except for K_2O (3.90 wt.% in AD60 and 2.88 wt.% in 98N50). Petrographic observations indicate that amphibole is a late crystallizing phase in the charnockitic facies and, when it is scarce, it only occurs as narrow rims around the pyroxenes and Fe-Ti oxides. On the other hand, in this facies, orthopyroxene is abundant and petrographic textures suggest its early crystallization. Accordingly, the 98N06 phase diagram indicates that the H_2O content must have been below 5 wt.% at the beginning of crystallization and reached about 6 wt.% near the solidus (Bogaerts et al., 2006). Assuming a fraction of liquid of 0.75 based on the modeling of the fractional crystallization, the H_2O content can thus be estimated at 4.5 wt.% at the liquidus of the charnockitic facies. This H_2O content probably represents a maximum value as comparison between the calculated and experimental cumulates indicates that in the charnockitic magma, the H_2O content was lower than in the experimental charge (4.2 wt.%). It is possible that the late crystallisation of amphibole in the charnockitic facies as rims around opaques or Fe-Mg silicates was due to an increased proportion of H_2O in the boundary layer close to the Fe-Mg silicates. The absence of orthopyroxene in the granitic facies imposes that the H_2O content was > 6 wt.% when amphibole crystallized (Bogaerts et al., 2006).

Considering an H_2O content of 6.5 wt.% in the liquid when its fraction was 0.75, an H_2O content higher than 5 wt.% can be estimated for the liquidus of the granitic facies taking into account the amount of H_2O present in the cumulate (amphibole, biotite). The good agreement between the calculated cumulate and the experimental one, which is in equilibrium with a melt containing 5.4 wt.% H_2O, supports this result. Not surprisingly, the charnockitic and granitic facies are characterized by different water contents. However, their different mineralogies probably also result from their different Fe# as an increase of the melt Fe# expands the stability field of orthopyroxene and shrinks that of amphibole and biotite (Naney, 1983; Frost and Frost, 2008a).

Given the estimated H_2O content of the parent magmas and the fraction of residual liquid calculated with the least square regression method (about 0.75), the H_2O content in the residual melt has been calculated to 6.1 wt.% H_2O and 6.4 wt.% in the charnockitic and granitic facies, respectively. In this calculation, the amount of H_2O present in the cumulate of the granitic facies (1.5 wt.% in the amphibole and 3 wt.% in the biotite) was taken into account. These values are well below H_2O saturation which is reached in these liquids at about 9.2 to 10 wt. % H_2O at 0.4 GPa according to the experimental data of Bogaerts et al. (2006). Consequently, second boiling and gas-driven filter processes (Anderson et al., 1984; Sisson and Bacon, 1999) have not occurred in the Farsund intrusion. Two lines of evidence indicate that most of the water initially present in the parent magmas was concentrated in the residual melts. First, the amount of water in the cumulates is negligible (less than 1 wt. % in the granitic facies: amphibole and biotite present in the subtracted cumulate, Table 6; anhydrous phases in the cumulates of the charnockitic facies, Table 6) and second, aplitic and pegmatitic dykes are very rare and usually of limited thickness (about 1 dm). The residual liquids were thus abundant (F = 0.75) and had low viscosities (high H_2O content and temperature, see Supplementary material). Given these properties, we suggest that they were able to leave the magma chamber and rise up to the surface of the Mesoproterozic continental crust to produce volcanism, an hypothesis already proposed by Bogaerts et al. (2003b) for the nearby Lyngdal intrusion and by Vander Auwera et al. (2008) for the granitoids of the HBG suite. This process potentially tranferred a significant amount of H_2O from the lower crust to the surface.

7. Conclusions

The Farsund intrusion was built up by the emplacement and mingling of two different broadly coeval magmas that belong to the two Sveconorwegian late-orogenic magmatic suites recognized in southern Norway: the HBG and AMC suites.

The geochemistry of the Farsund body was controlled by its location close to both the opx-in isograd of the Sveconorwegian regional metamorphism and the Farsund-RAP shear zone that separates two different lithotectonic units. The charnockitic facies displaying the petrographic and geochemical characteristics of the AMC suite (opx-bearing) also bear evidence of the C1 component characterized by relatively radiogenic Sr (0.7097-0.7111) and Pb isotopes, combined with epsilon-Nd values scattered around zero whereas the granitic facies having the signature of the HBG suite (abundant hornblende) show isotopic signatures of the C2 component characterized by significantly lower Sr isotope ratios (0.70540.7078) and less radiogenic Pb isotopes, associated with mildly negative epsilon-Nd values (ca. -1). It is also very likely that the Farsund-RAP shear zone favored the ascent and emplacement of the Farsund magmas.

Taken as a whole, mineral composition, geochemical and isotopic data clearly indicate that the two magmas did not mix during rise through the crust, final emplacement and crystallization at about 0.4 GPa, thus further suggesting that these processes were fast in agreement with the rather low viscosities of the magmas. Moreover, the isotopic composition of the two magmas was modified in the lower crustal source by bulk assimilation of the C1 or C2 components. These data support recent models suggesting that granitic bodies are built by multiple batches of magmas derived from contrasting sources. Modeling of the differentiation shows that fractional crystallization can predict the observed trends in both magmas and indicates that a limited extent of differentiation occurred in the shallow magma chamber. It was also speculated that part of the rather H_2O-rich residual melts could have erupted on the Mesoproterozoic continental crust thus contributing to the transfer of H_2O from the lower crust to the atmosphere.

Acknowledgements

This work was funded by the Belgian Fund for scientific research (FNRS), the Research Funds of the University of Liège and A.D. received a FRIA PhD fellowship. G. Bologne is thanked for the assistance with X-ray fluorescence and ICPMS analyses. An earlier version of the manuscript has been improved thanks to the constructive comments of B. Bonin and S. Erdmann. Detailed comments and helpful suggestions provided by two anonymous reviewers were greatly appreciated.

References

Andersen, T., Andresen, A., Sylvester, A., 2001. Nature and distribution of deep crustal reservoirs in the southwestern part of the Baltic shield: evidence from Nd, Sr and Pb isotope data on late Sveconorwegian granites. Journal of the Geological Society 158, 253-267.

Andersen, T., Andresen, A., Sylvester, A., 2002. Timing of late- to post-tectonic Sveconorwegian granitic magmatism in South Norway. Norges geologiske undersøkelse Bulletin 440, 5-18.

Andersen, T., Graham, S., Sylvester, A.G., 2007. Timing and tectonic significance of Sveconorwegian A-type granitic magmatism in Telemark, southern Norway: new results from laser-ablation ICPMS U-Pb dating of zircon. Norges Geologiske

Undersøkelse Bulletin 447, 17-31.

Andersen, T., Hagelia, P., Whitehouse, M.J., 1994. Precambrian multi-stage crustal evolution in the Bamble sector of south Norway: Pb isotopic evidence from a Sveconorwegian deep-seated granitic intrusion. Chemical Geology (Isotope Geoscience Section) 116, 327-343.

Andersen, T., Maijer, C., Veschure, R.H., 1995. Metamorphism, provenance ages and source characteristics of Precambrian clastic metasediments in the Bamble sector, south Norway. Petrology 3, 321-339.

Andersen, T., Sundvoll, B., 1995. Neodymium isotope systematics of the mantle beneath the Baltic shield: evidence for depleted mantle evolution since the Archaean. Lithos 35, 235-243.

Anderson, A.T.J., Swihart, G.H., Artioli, G., Geiger, C.A., 1984. Segregation vesicles, gas filter-pressing, and igneous differentiation. Journal of Geology 92, 55-72.

Andersson, M., Lie, J., Husebye, E., 1996. Tectonic setting of post-orogenic granites within SW Fennoscandia based on deep seismic and gravity data. Terra Nova 8, 558-566.

Annen, C., Blundy, J.D., Sparks, R.S.J., 2006. The genesis of intermediate and silicic magmas in Deep crustal hot zones. Journal of Petrology 47, 505-539.

Bacon, C.R., Druitt, T.H., 1988. Compositional evolution of the zoned calc-alkaline magma chamber of Mount Mazama, crater Lake, Oregon. Contributions to Mineralogy and Petrology 98, 224-256.

Barbarin, B., Didier, J., 1992. Genesis and evolution of mafic microgranular enclaves through various types of interaction between coexisting felsic and mafic magmas. Transactions of the Royal Society of Edinburgh, Earth Sciences 83, 145-153.

Barker, F., 1979. Trondhjemite: Definition, environment and hypotheses of origin. In: Barker, F. (Ed.), Trondhjemites, dacites and related rocks. Elsevier, Amsterdam, pp. 1-12.

Barling, J., Weis, D., Demaiffe, D., 2000. A Sr-, Nd-, and Pb-isotopic investigation of the transition between two megacyclic units of the Bjerkreim-Sokndal layered intrusion, south Norway. Chemical Geology 165, 47-65.

Bea, F., Pereira, M., Stroh, A., 1994. Mineral/leucosome trace-element partitioning in a peraluminous migmatite (a laser ablation-ICP-MS study). Chemical Geology 117, 291-312.

Beard, J.S., Lofgren, G.E., 1991. Dehydration melting and water-saturated melting of basaltic and andesitic greenstones and amphibolites a 1, 3, 6.9 kb. Journal of Petrology 32, 365-401.

Bingen, B., Davis, W., Hamilton, M., Engvik, A., Stein, H., Skar, Ø., Nordgulen, Ø., 2008a. Geochronology of high-grade metamorphism in the Sveconorwegian belt, South Norway: U-Pb, Th-Pb and Re-Os data. Norwegian Journal of Geology 88, 13-42.

Bingen, B., Nordgulen, Ø., Viola, G., 2008b. A four-phase model for the Sveconorwegian orogeny, SW Scandinavia. Norwegian Journal of Geology 88, 43-72.

Bingen, B., Skår, Ø., Marker, M., Sigmond, E.M.O., Nordgulen, Ø., Ragnhildsveit, J., Mansfeld, J., Tucker, R.D., Liégeois, J.-P., 2005. Timing of continental building in the Sveconorwegian orogen, SW Norway. Norwegian Journal of Geology 85, 87-116.

Bingen, B., Stein, H.J., Bogaerts, M., Bolle, O., Mansfeld, J., 2006. Molybdenite Re-Os dating constrains gravitational collapse of the Sveconorwegian orogen, SW Scandinavia. Lithos 87, 328-346.

Bingen, B., van Breemen, O., 1998. U-Pb monazite ages in amphibolite- to granulite-facies orthogneisses reflect hydrous mineral breakdown reactions: Sveconorwegian Province of SW Norway. Contributions to Mineralogy and Petrology 132, 336-353.

Bogaerts, M., Scaillet, B., Liégeois, J.-P., Vander Auwera, J., 2003a. Petrology and geochemistry of the Lyngdal granodiorite (Southern Norway) and the role of fractional crystallization in the genesis of the Proterozoic ferro-potassic A-type granites. Precambrian Research 124, 149-184.

Bogaerts, M., Scaillet, B., Vander Auwera, J., 2003b. Emplacement of the Lyngdal granodiorite (SW Norway) at the brittle-ductile transition in a hot crust. Joint EGS-EUG. Cambridge University Publications, Nice (France), p. 03611.

Bogaerts, M., Scaillet, B., Vander Auwera, J., 2006. Phase equilibria of the Lyngdal granodiorite (Norway) : Implications for the origin of metaluminous ferroan granitoids. Journal of Petrology 47, 2405-2431.

Bogdanova, S., Bingen, B., Gorbatschev, R., Kheraskova, T., Kozlov, V., Puchkov, V., Volozh, Y., 2008. The East European Craton (Baltica) before and during the assembly of Rodinia. Precambrian Research 160, 23-45.

Bolle, O., Demaiffe, D., Duchesne, J.C., 2003a. Petrogenesis of jotunitic and acidic members of an AMC suite (Rogaland anorthosite province, SW Norway): a Sr and Nd isotopic assessment. Precambrian Research 124, 185-214.

Bolle, O., Diot, H., Trindade, R.I.F., 2003b. Magnetic fabrics in the Holum granite (Vest-Agder, southernmost Norway): implications for the late evolution of the Sveconorwegian (Grenvillian) orogen of SW Scandinavia. Precambrian Research 121, 221-249.

Bolle, O., Diot, H., Liégeois, J.-P., Vander Auwera, J., 2010. The Farsund intrusion (SW Norway): a marker of Late-Sveconorwegian (Grenvillian) coeval transtension and gravity-driven tectonism. Journal of Structural Geology 32, 1500-1518.

Bolle, O., Duchesne, J.C., 2007. The Apophysis of the Bjerkreim-Sokndal layered intrusion (Rogaland anorthosite province, SW Norway): a composite pluton build up by tectonically-driven emplacement of magmas along the margin of an AMC igneous complex. Lithos 98, 292-312.

Buddington, A., 1959. Granite emplacement with special reference to North America. Geological Society of America Bulletin 70, 671-747.

Charlier, B., Duchesne, J.C., Vander Auwera, J., Storme, J.Y., Maquil, R., Longhi, J., 2010. Polybaric fractional crystallization of high-alumina basalt parental magmas in the Egersund-Ogna massif-type anorthosite (Rogaland, SW Norway) constrained by plagioclase and high-alumina orthopyroxene megacrysts. Journal of Petrology 51, 2515-2546.

Clemens, J.D., Helps, P.A., Stevens, G., 2009. Chemical structure in granitic magmas - A signal from the source? Earth and Environmental Science Transactions of the Royal Society of Edinburgh 100, 159-172.

Clemens, J.D., Stevens, G., 2012. What controls chemical variation in granitic magmas? Lithos 134-135, 317-329.

Dekker, A.G., 1978. Amphiboles and their host rocks in the high-grade metamorphic Precambrian of Rogaland/Vest-Agder, SW. Norway. Rijksuniversiteit te Utrecht, Utrecht.

Demaiffe, D., Bingen, B., Wertz, P., Hertogen, J., 1990. Geochemistry of the Lyngdal hyperites (S.W. Norway): comparison with the monzonorites associated with the Rogaland anorthosite complex. Lithos 24, 237-250.

Demaiffe, D., Weis, D., Michot, J., Duchesne, J.C., 1986. Isotopic constraints on the genesis of the anorthosite suite of rocks. Chemical Geology 57, 167-179.

Duchesne, J.C., 2001. The Rogaland Intrusive Massifs- an excursion guide. NGU Report 2001.29, Geological Survey of Norway.

Duchesne, J.C., Liégeois, J.-P., Bolle, O., Vander Auwera, J., Bruguier, O., Matukov, D.I., Sergeev, S., 2013. The fast evolution of a crustal hot zone at the end of a transpressional regime: The Saint-Tropez peninsula granites and related dykes (Maures Massif, SE France). Lithos 162-163, 195-220.

Duchesne, J.C., Wilmart, E., 1997. Igneous charnockites and related rocks from the Bjerkreim-Sokndal layered intrusion (Southwest Norway): a jotunite (hypersthene monzodiorite)-derived A-type granitoid suite. Journal of Petrology 38, 337-369.

Dupont, A., 2004. Pétrologie, géochimie et géochimie isotopique du massif de Farsund (Norvège): implications pour le magmatisme AMCG. Université de Liège, Liège, pp. 279.

Dupont, A., Vander Auwera, J., Paquette, J.-L., Pin, C., Bogaerts, M., 2005. Inefficiency of magma mixing and source heterogeneity in the genesis of granitoids: the example of the Farsund body (southern Norway). Joint EGS-EUG. Cambridge Publications, Nice (France).

Emslie, R.F., Hamilton, M.A., Thiérault, R.J., 1994. Petrogenesis of a Mid-Proterozoic Anorthosite - Mangerite - Charnockite - Granite (AMCG) complex: isotopic and chemical evidence from the Nain plutonic suite. Journal of Geology 102, 539-558.

Ewart, A., Griffin, W., 1994. Application of proton-microprobe data to trace-element partitioning in volcanic rocks. Chemical Geology 117, 251-284.

Falkum, T., 1982. Geologisk kart over Norge, berggrunnskart Mandal - 1:250000, Norges Geologiske Undersøkelse.

Falkum, T., 1998. The Sveconorwegian magmatic and tectonometamorphic evolution of the high-grade Proterozoic Flekkefjord complex. Norges Geologiske Undersøkelse Bulletin 434, 5-33.

Falkum, T., Petersen, J., 1974. A three-fold division of the "farsundite" plutonic complex at Farsund, southern Norway. Norsk Geologisk Tidsskrift 54, 361-366.

Falkum, T., Wilson, J., Annis, M., Fregerslev, S., Zimmermann, H., 1972. The intrusive granites of the Farsund area, South Norway. Norsk Geologisk Tidsskrift 52, 463-465.

Falkum, T., Wilson, J., Petersen, J., Zimmermann, H., 1979. The intrusive granites of the Farsund area, south Norway: their interrelations and relations with the Precambrian metamorphic envelope. Norsk Geologisk Tidsskrift 59, 125-139.

Faure, G., 1986. Principles of isotope geology. Wiley, New York, pp. 589.

Fram, M., Longhi, J., 1992. Phase equilibria of dikes associated with Proterozoic anorthosite complexes. American Journal of Science 77, 605-616.

Frost, B.R., Frost, C.D., 2008a. On charnockites. Gondwana Research 13, 30-44.

Frost, B.R., Frost, C.D., 2008b. A geochemical classification for feldspathic igneous rocks. Journal of Petrology 49, 1955-1969.

Frost, B.R., Arculus, R.J., Barnes, C.G., Collins, W.J., Ellis, D.J., Frost, C.D., 2001. A geochemical classification of granitic rock suites. Journal of Petrology 42, 2033-2048.

Fujimaki, H., 1986. Partition coefficients of Hf, Zr, and REE between zircon, apatite and liquid. Contributions to Mineralogy and Petrology 94, 42-45.

Glazner, A.F., Bartley, J.M., Coleman, D.S., Gray, W., Taylor, R.Z., 2004. Are plutons assembled over millions of years by amalgamation from small magma chambers? GSA Today 14, 4-11.

Harrison, T.M., Watson, E.B., 1984. The behavior of apatite during crustal anatexis: equilibrium and kinetic considerations. Geochimica et Cosmichimica Acta 48, 1467-1477.

Henry, D.J., Guidotti, C.V., Thomson, J.A., 2005. The Ti-saturation surface for low-to-medium pressure metapelitic biotites: implications for geothermometry and Ti-substitution mechanisms. American Mineralogist 90, 316-328.

Jacobsen, S., Wasserburg, G.J., 1980. Sm-Nd isotopic evolution of chondrites. Earth and Planetary Science Letters 50, 139-155.

Johnson, M.C., Rutherford, M.J., 1989. Experimental calibration of the aluminium in hornblende geobarometer with application to Long Valley caldera (California) volcanic rocks. Geology 17, 837-841.

Knudsen, T., Andersen, T., Maijer, C., Verschure, R., 1997. Trace-element characteristics and Pb isotopic evolution of metasediments and associated Proterozoic rocks from the amphibolite- to granulite-facies Bamble sector, southern Norway. Chemical Geology 143, 145-169.

Kolderup, C., 1903. Die Labradorfelse des westlichen Norwegens. II. Die Labradorfelse und die mit densebelden verwandten Gesteine in dem Bergensgebiete. Bergens Museums Aarbog Afhandlinger og Arsberetning 12, 1-129.

Longhi, J., Vander Auwera, J., Fram, M., Duchesne, J.C., 1999. Some phase equilibrium constraints on the origin of Proterozoic (Massif) anorthosites and related rocks. Journal of Petrology 40, 339-362.

Mahood, G., Hildreth, E., 1983. Large partition coefficients for trace elements in high-silica rhyolites. Geochimica et Cosmochimica Acta 47, 11-30.

Mahood, G., Stimac, J., 1990. Trace element partitioning in pantellerites and trachytes. Geochimica et Cosmochimica Acta 54, 257-276.

Marker, M., Schiellerup, H., Meyer, G.B., Robins, B., Bolle, O., 2003. Geological map of the Rogaland anorthosite province - scale 1:75000. In: Duchesne, J.C., Korneliussen, A. (Eds.), Ilmenite Deposits and Their Geological Environment. With Special Reference to the Rogaland Anorthosite Province.

McKay, G., 1989. Partitioning of rare earth elements between major silicate minerals and basaltic melts. In: Lipin, B., McKay, G. (Eds.), Geochemistry and mineralogy of REE. Mineralogical Society of America, Reviews in Mineralogy, 21, pp. 45-77.

Menuge, J., 1988. The petrogenesis of massif anorthosites: a Nd and Sr isotopic investigation of the Proterozoic of Rogaland-Vest Agder, SW Norway. Contributions to Mineralogy and Petrology 98, 363-373.

Middlemost, E., 1968. The granitic rocks of Farsund, south Norway. Norsk Geologisk Tidsskrift 48, 81-99.

Miller, R., Paterson, S., 1999. In defense of magmatic diapirs. Journal of Structural Geology 21, 1161-1173.

Miyashiro, A., 1978. Nature of alkalic volcanic rock series. Contributions to Mineralogy and Petrology 66, 91-104.

Morimoto, N., 1989. Nomenclature of pyroxenes. Canadian Mineralogist 27, 143-156.

Nagasawa, H., 1973. Rare earth distribution in alkali rocks from Oki-Dogo Island, Japan. Contributions to Mineralogy and Petrology 39, 301-308.

Nagasawa, H., Schnetzler, C., 1971. Partitioning of rare earth, alkali, and alkaline earth elements between phenocrysts and acidic igneous magmas. Geochimica et Cosmochimica Acta 35, 953-968.

Nakamura, Y., Fujimaki, H., Nakamura, N., Tatsumoto, M., 1986. Hf, Zr, and REE partition coefficients between ilmenite and liquid: implications for lunar petrogenesis. Proceedings of the 16th Lunar and Planetary Science Conference, D239-D250.

Naney, M., 1983. Phase equilibria of rock-forming ferromagnesian silicates in granitic systems. American Journal of Science 283, 993-1033.

Nash, W., Crecraft, H., 1985. Partition coefficients for trace elements in silicic magmas. Geochimica et Cosmochimica Acta 49, 309-322.

Pasteels, P., Demaiffe, D., Michot, J., 1979. U-Pb and Rb-Sr geochronology of the eastern part of the South Rogaland igneous complex, southern Norway. Lithos 12, 199-208.

Petersen, J., 1980. Rare-Earth Element fractionation and petrogenetic modelling in charnockitic rocks, southwest Norway. Contributions to Mineralogy and Petrology 73,

161-172.
Petford, N., Cruden, A., McCaffrey, K., Vigneresse, J.-L., 2000. Granite magma formation, transport and emplacement in the Earth's crust. Nature 408, 669-673.
Pressley, R., Brown, M., 1999. The Phillips pluton, Maine, USA: evidence of heterogeneous crustal sources and implications for granite ascent and emplacement mechanisms in convergent orogens. Lithos 46, 335-366.
Putirka, K.D., 2008. Thermometers and barometers for volcanic systems. In: Putirka, K.D., Tepley, F.J. (Eds.), Minerals, inclusions and volcanic rocks. Mineralogical Society of America, Reviews in Mineralogy, 69, pp. 61-120.
Rajesh, H., 2007. The petrogenetic characterization of intermediate and silicic charnockites in high-grade terrains: a case study from southern India. Contributions to Mineralogy and Petrology 154, 591-606.
Rajesh, H., 2012. A geochemical perspective on charnockite magmatism in Peninsular India. Geoscience Frontiers 3, 773-788.
Rajesh, H., Santosh, M., 2004. Charnockitic magmatism in southern India. Proceedings of the Indian Academy of Sciences, Earth and Planetary Sciences 113, 565-585.
Reid, F., 1983. Origin of the rhyolitic rocks of the Taupo volcanic zone, New Zealand. Journal of Volcanology and Geothermal Research 15, 315-338.
Romer, R.L., Heinrich, W., Schröder-Smeibidl, B., Meixner, A., Fischer, C.-O., Schulz, C., 2005. Elemental dispersion and stable isotope fractionation during reactive fluid-flow and fluid immiscibility in the Bufa del Diente aureole, NE-Mexico: evidence from radiographies and Li, B, Sr, Nd, and Pb isotope systematics. Contributions to Mineralogy and Petrology 149, 400-429.
Rosenberg, P.E., Foit, F.F., Jr, 1977. Fe2+-F avoidance in silicates. Geochimica et Cosmochimica Acta 41, 345-346.
Sano, Y., Terada, K., Fukuoka, T., 2002. High mass resolution ion microprobe analysis of rare earth elements in silicate glass, apatite and zircon: lack of matrix dependency. Chemical Geology 184, 217-230.
Schärer, U., Wilmart, E., Duchesne, J.C., 1996. The short duration and anorogenic character of anorthosite magmatism: U-Pb dating of the Rogaland Complex, Norway. Earth and Planetary Science Letters 139, 335-350.
Schiellerup, H., Lambert, R., Prestvik, T., Robins, B., McBride, J., Larsen, R., 2000. Re-Os isotopic evidence for a lower crustal origin of massif-type anorthosites. Nature 405, 781-784.
Sisson, T., 1994. Hornblende-melt trace element partitioning measured by ion microprobe. Chemical Geology 117, 331-344.
Sisson, T., Ratajeski, K., Hankins, W., Glazner, A., 2005. Voluminous granitic magmas from common basaltic sources. Contributions to Mineralogy and Petrology 148, 635-661.
Sisson, T., 1991. Pyroxene-High Silica rhyolite trace-element partition coefficients measured by ion microprobe. Geochimica et Cosmochimica Acta 55, 575-585.
Sisson, T., Bacon, C.R., 1999. Gas-driven filter in magmas. Geology 27, 613-616.
Solano, J., Jackson, M., Sparks, R., Blundy, J.D., Annen, C., 2012. Melt segregation in deep crustal hot zones: a mechanism for chemical differentiation, crustal assimilation and the formation of evolved magmas. Journal of Petrology 53, 1999-2026.
Stacey, J., Kramers, J., 1975. Approximation of terrestrial lead isotope evolution by a two-stage model. Earth and Planetary Science Letters 26, 207-221.
Steiger, R., Jäger, E., 1977. Subcommission on geochronology: convention on the use of decay constants in geo- and cosmochronology. Earth and Planetary Sciences Letters 36, 359-362.

Streck, M., Grunder, A., 1997. Compositional gradients and gaps in high-silica rhyolites of the Rattlesnake Tuff, Oregon. Journal of Petrology 38, 133-163.

Streckeisen, A., 1974. How should charnockitic rocks be named? Société Géologique de Belgique Géologie des domaines cristallins, 349-360.

Sun, S., McDonough, W., 1989. Chemical and isotopic systematics of oceanic basalts: implications for mantle composition and processes. In: Saunders, A., Norry, M. (Eds.), Magmatism in the ocean basins. Blackwell Scientific publications, pp. 313-345.

Tanaka, T., Togashi, S., Kamioka, H., Amakawa, H., Kagami, H., Hamamoto, T., Yuhara, M., Orihashi, Y., Yoneda, S., Shimizu, H., Kunimaru, T., Takahashi, Y., Yanagi, T., Nakano, T., Fujimaki, H., Shinjo, R., Asahara, Y., Tanimizu, M., Dragusanu, C., 2000. JNdi-1: a neodymium isotopic reference in consistency with LaJolla neodymium. Chemical Geology 168, 279-281.

Toplis, M., Corgne, A., 2002. An experimental study of element partitioning between magnetite, clinopyroxene and iron-bearing silicate liquids with particular emphasis on vanadium. Contributions to Mineralogy and Petrology 144, 22-37.

Vander Auwera, J., Bogaerts, M., Bolle, O., Longhi, J., 2008. Genesis of intermediate igneous rocks at the end of the Sveconorwegian (Grenvillian) orogeny (S Norway) and their contribution to intracrustal differentiation. Contributions to Mineralogy and Petrology 156, 721-743.

Vander Auwera, J., Bogaerts, M., Liégeois, J.-P., Demaiffe, D., Wilmart, E., Bolle, O., Duchesne, J.C., 2003. Derivation of the 1.0-0.9 Ga ferro-potassic A-type granitoids of southern Norway by extreme differentiation from basic magmas. Precambrian Research 124, 107-148.

Vander Auwera, J., Bolle, O., Bingen, B., Liégeois, J.-P., Bogaerts, B., Duchesne, J.C., De Waele, B., Longhi, J., 2011. Sveconorwegian massif-type anorthosites and related granitoids result from post-collisional melting of a continental arc root. Earth-Science Reviews 107, 375-397.

Vander Auwera, J., Longhi, J., Duchesne, J.C., 1998. A liquid line of descent of the jotunite (hypersthene monzodiorite) suite. Journal of Petrology 39, 439-468.

Vigneresse, J.-L., 2004. A new paradigm for granite generation. Transactions of the Royal Society of Edinburgh-Earth Sciences 95, 11-22.

Villemant, B., 1988. Trace element evolution in the Phlegrean fields (central Italy) - Fractional crystallization and selective enrichment. Contributions to Mineralogy and Petrology 98, 169-183.

Watson, E.B., Harrison, T.M., 1983. Zircon saturation revisited: temperature and compositional effects in a variety of crustal magma types. Earth and Planetary Science Letters 64, 295-304.

Weis, D., 1986. Genetic implications of Pb isotope geochemistry in the Rogaland anorthositic complex (southwest Norway). Chemical Geology 57, 181-199.

Whalen, J.B., Currie, K.L., Chappell, B.W., 1987. A-type granites: geochemical characteristics, discrimination and petrogenesis. Contributions to Mineralogy and Petrology 95, 407-419.

Wiebe, R.A., 1984. Commingling of magmas in the Bjerkreim-Sokndal lopolith (southwest Norway): evidence for the compositions of residual liquids. Lithos 17, 171-188.

Wilson, J., Robins, B., Nielsen, F., Duchesne, J.C., Vander Auwera, J., 1996. The Bjerkreim-Sokndal layered intrusion, Southwest Norway. In: Cawthorn, R. (Ed.), Layered Intrusions. Elsevier, Amsterdam, pp. 231-256.

Figures captions

Fig. 1. (A) Situation map of SW Scandinavia and of the Sveconorwegian orogen with its N-S trending crustal discontinuities (Bingen et al., 2005; Bingen et al., 2008b). (B) Geological sketch map of SW Scandinavia showing the Sveconorwegian late-orogenic magmatic suites as well as the orogenic granitoids. F: Farsund, Sj: Sjelset, Ly: Lyngdal, K: Kleivan, Sv: Svöfjell. The position of the opx-in isograd related to the Sveconorwegian regional metamorphism is also shown by dotted lines and crosses (after Bingen et al., 2008b).

Fig. 2. Geological sketch map of southwest Rogaland showing the Rogaland Anorthosite Province (RAP) and the location of the Farsund, Kleivan (K), Lyngdal (L), Tranevåg (T), Bjerkreim-Sokndal (BKSK), Apophysis (A) and Hidra (H) intrusions. The location of the Farsund-RAP shear zone (strongly-foliated rocks shown as a ruled band) and the opx-in isograd are also displayed (after Falkum, 1982; Bingen et al., 2006; Bolle et al., 2010).

Fig. 3. Distribution of the facies of the Farsund intrusion (after Bolle et al., 2010) (J = Jøllestø location). Samples that were grouped in the granitic facies because of their very low amount of orthopyroxene are included in the HBG domain (see section 3.1. for explanation). AMS (Bolle et al., 2010) and geochemistry (Dupont, 2004) sampling sites are located. At some locations, two samples were collected, one for the AMS study and another for geochemistry, but only one point is shown on this map. The contours of the large gneissic body located in the center of the intrusion are also shown.

Fig. 4. (A) Opx-bearing hornblendites in the coarse grained quartz monzonite at Jøllestø. (B) Enclave of banded gneiss. Photomicrographs (transmitted light) of sample AD017 (charnockitic facies) in parallel (C) and crossed (D) nicols and of sample AD060 (granitic facies) in parallel (E) and crossed (F) nicols (Hbl = hornblende, Op = opaques, Ttn = titanite, Ap = apatite, Zrn = zircon, Opx = orthopyroxene, Inv Pgt = inverted pigeonite, Qtz = quartz, Pl = plagioclase).

Fig. 5. Major elements compositional variations of amphibole (A-B), orthopyroxene (C), clinopyroxene (D) and biotite (E-F) in the charnockitic (filled circles) and granitic (open circles) facies of the Farsund intrusion (data from Dupont (2004) and this study) compared to mineral compositions observed in the AMC (data from Dekker (1978); Wiebe (1984); Bolle and Duchesne (2007) and this study) and HBG (data from Bogaerts et al. (2003a); Bolle et al. (2003b); Vander Auwera et al. (2003) and this study) suites. Average mineral analyses are plotted.

Fig. 6. Nomenclature of the Farsund facies in the Fe#-index ($FeO_t/(FeO_t+MgO)$ diagram (revised boundary with total iron of Frost and Frost (2008b)) (A) and MALI ($Na_2O+ K_2O-CaO$) diagram (B) of Frost et al. (2001) and Frost and Frost (2008b), in the TAS diagram (Na_2O+K_2O versus SiO_2) (C) with the discrimination curve of Miyashiro (1978) and in the ASI (Al/(Ca-1.67P+Na+K)) diagram (D) of Frost et al. (2001).

Fig. 7. Classification of the Farsund rocks according to their CIPW normative composition (same symbols as in Fig. 6) (Barker, 1979).

Fig. 8. Major elements composition of the Farsund facies compared with the AMC suite (OLT, PXT for the upper part of the Bjerkreim-Sokndal intrusion (Duchesne and Wilmart, 1997); APT for the Apophysis (Bolle and Duchesne, 2007)) and HBG suite (Svöfjell, Lyngdal, Tranevåg: Demaiffe et al. (1990); Bogaerts et al. (2003a); Vander Auwera et al. (2003)).

Fig. 9. Trace elements composition of the Farsund facies compared with the trace elements composition of the AMC and HBG suites (same data as in Fig. 8). Same symbols as in Fig. 6.

Fig. 10. REE patterns of the charnockitic and granitic facies of the Farsund intrusion compared with the REE patterns observed in the Lyngdal intrusion (HBG suite: data from Bogaerts et al. (2003a)) and in the Apophysis of the Bkjerkreim-Sokndal intrusion (AMC suite: data from Bolle and Duchesne (2007)). REE data of Petersen (1980) for the Farsund

intrusion are shown in the grey field. Samples normalized to the chondrite C1 of Sun and McDonough (1989).

Fig. 11. U-Pb data on zircon from samples AD017 (charnockitic facies) and AD060 (granitic facies) of the Farsund intrusion. See Table 3.

Fig. 12. Initial Sr, Nd (A) and Pb (B) isotopic compositions of the Farsund facies compared with data from the HBG and AMC suites. Isotopic compositions have been recalculated back to the emplacement age of the Farsund intrusion (0.93 Ga). Sr and Nd isotopic data from Demaiffe et al. (1990), Andersen et al. (2001), Bogaerts et al. (2003a), Vander Auwera et al. (2003) and this study. Pb isotopic data from Weis (1986), Demaiffe et al. (1990), Barling et al. (2000), Andersen et al. (2001) and this study. Evolution of Bulk Silicate Earth (BSE) is calculated back from present ratios of $^{87}Sr/^{86}Sr = 0.7047$ and $^{87}Rb/^{86}Sr = 0.0850$ (Faure, 1986). Same symbols as in Fig. 6. Crosses in Fig. 12B are data from Weis (1986) for the Farsund intrusion (a detailed description was not given for these samples, thereby precluding their assignment to the two facies recognised in this work).

Highlights

The Farsund intrusion is made of two intermingled coeval facies.

The two facies belong to the two Sveconorwegian late-orogenic magmatic suites.

The Farsund intrusion was emplaced close to a shear zone and the opx-in isograd.

Limited differentiation occurred within each facies in the upper crust.

Table 1: Sample number, location and facies

Sample #	UTM-x	UTM-y	Ferromagnesian minerals	Facies	Rock name
	(*ital. = map* ; reg=GPS)				
MB9914	*0360250*	*6448300*	Hbl, Bt, no Opx	Granitic	Qtz monzonite
MB9915	*0360250*	*6448300*	Hbl, Bt, no Opx	Granitic	Qtz monzonite
MB9927	0361779	6447490	Hbl, Bt, no Opx	Granitic	Qtz monzonite
AD004	0362517	6449402	Hbl, Bt, no Opx	Granitic	Qtz monzonite
AD016	*0366125*	*6445910*	Hbl, Bt, no Opx	Granitic	Qtz monzodiorite
AD057	0359555	6447557	Hbl, Bt, no Opx	Granitic	Qtz monzonite
AD058	0359833	6448463	Hbl, Bt, no Opx	Granitic	Granite
AD060	0359926	6448500	Hbl, Bt, no Opx	Granitic	Qtz monzodiorite
AD061	0361920	6450535	Hbl, Bt, no Opx	Granitic	Qtz monzonite
AD063	0365855	6446406	Hbl, Bt, no Opx	Granitic	Qtz monzonite
FA85	0366391	6446949	Hbl, Bt, no Opx	Granitic	Qtz monzonite
98N20	*0358985*	*6446770*	Hbl, some Opx	Granitic	Qtz monzonite
98N21	0358782	6446644	Hbl, some Opx	Granitic	Monzonite
98N22	0358782	6446644	Hbl, some Opx	Granitic	Hornblendite
98N23	0358782	6446644	Hbl, some Opx	Granitic	Qtz monzonite
98N24	0358782	6446644	Hbl, some Opx	Granitic	Qtz monzonite
98N25	0358782	6446644	Hbl, some Opx	Granitic	Qtz monzonite
MB9910	0358782	6446644	Hbl, some Opx	Granitic	Monzonite
MB9911	0358782	6446644	Hbl, some Opx	Granitic	Qtz monzonite
MB9912	0358782	6446644	Hbl, some Opx	Granitic	Granite
MB9913	0358782	6446644	Hbl, some Opx	Granitic	Hornblendite
AD018	0358782	6446644	Hbl, some Opx	Granitic	Qtz monzonite
AD029	*0359140*	*6455675*	Hbl, some Opx	Granitic	Qtz monzonite
AD033	0359159	6455734	Hbl, some Opx	Granitic	Monzonite
AD066	0361353	6446774	Hbl, some Opx and Bt	Granitic	Qtz monzonite
AD067	0358782	6446644	Hbl, some Opx	Granitic	Hornblendite
FA68	0359360	6453972	Hbl, some Opx and Bt	Granitic	Qtz monzonite
FA71	0359571	6447494	Hbl, some Opx	Granitic	Granite
FA102	0365108	6452728	Hbl, some Opx	Granitic	Qtz monzonite
98N26	*0360685*	*6450850*	Hbl>Opx	Charnockitic	Charnockite
98N60	*0372020*	*6444690*	Hbl>Opx	Charnockitic	Opx-bearing Qtz monzonite
MB9925	*0364365*	*6446500*	Hbl>Opx	Charnockitic	Opx-bearing Qtz monzonite
MB9935	0371236	6446617	Hbl>Opx	Charnockitic	Charnockite
AD006	0367670	6446339	Hbl>Opx	Charnockitic	Opx-bearing Qtz monzonite
AD026	0359523	6453407	Hbl>Opx	Charnockitic	Charnockite
AD037	0361952	6453775	Hbl>Opx	Charnockitic	Charnockite
FA17	0362130	6450219	Hbl>Opx	Charnockitic	Opx-bearing Qtz monzonite
FA81	0364786	6449343	Hbl>Opx	Charnockitic	Opx-bearing Qtz monzonite
FA113	0369433	6445217	Hbl>Opx	Charnockitic	Opx-bearing Qtz monzonite
98N19	*0371975*	*6441900*	Opx>Hbl	Charnockitic	Opx-bearing Qtz monzonite
98N28	*0366860*	*6450975*	Opx>Hbl	Charnockitic	Charnockite
98N58	*0368055*	*6443200*	Opx>Hbl	Charnockitic	Charnockite
98N59	*0369650*	*6444015*	Opx>Hbl	Charnockitic	Charnockite
MB9916	*0364685*	*6450525*	Opx>Hbl	Charnockitic	Opx-bearing Qtz monzonite
AD001	0358782	6446644	Opx>Hbl	Charnockitic	Charnockite
AD002	*0370640*	*6441510*	Opx>Hbl	Charnockitic	Opx-bearing Qtz monzonite
AD003	*0370860*	*6448625*	Opx>Hbl	Charnockitic	Opx-bearing Qtz monzonite
AD005	0369719	6448625	Opx>Hbl	Charnockitic	Charnockite
AD009	*0363710*	*6445750*	Opx>Hbl	Charnockitic	Opx-bearing Qtz monzonite
AD010	*0362935*	*6444900*	Opx>Hbl	Charnockitic	Charnockite
AD011	*0369025*	*6441800*	Opx>Hbl	Charnockitic	Opx-bearing Qtz monzonite
AD012	0369521	6442711	Opx>Hbl	Charnockitic	Opx-bearing Qtz monzonite
AD014	*0366840*	*6443375*	Opx>Hbl	Charnockitic	Charnockite
AD015	*0366460*	*6444035*	Opx>Hbl	Charnockitic	Opx-bearing Qtz monzonite
AD017	0359915	6445998	Opx>Hbl	Charnockitic	Charnockite
AD023	0358227	6454236	Opx>Hbl	Charnockitic	Charnockite
AD034	0362772	6456819	Opx>Hbl	Charnockitic	Opx-bearing Qtz monzonite
AD035	0362847	6456376	Opx>Hbl	Charnockitic	Opx-bearing Qtz monzonite
AD040	0360011	6457227	Opx>Hbl	Charnockitic	Charnockite

*samples in italic were analysed by microprobe; underlined samples were not analysed with XRF and ICPMS.
FA85, FA17, FA68, FA71, FA81, FA102, FA113 are from Bolle et al (2010).
Rock names are from modal compositions.
The fourth column gives the relative proportions of ferromagnesian minerals and the fifth column, the facies to which the sample belongs. See section 3 in the text.

Table 2: Major and trace element analyses of the Farsund samples

Sample no.	MB9913	AD067	MB9910	98N21	AD060	MB9914	AD061	MB9915	AD066	AD063	AD033	MB9911
Facies	Gr.	Gr.	Gr.	Gr.	Gr.	Gr.	Gr.	Gr.	Gr.	Gr.	Gr.	Gr.
SiO_2	36.23	44.67	57.94	58.42	59.87	60.95	61.99	62.45	62.48	62.52	62.92	63.11
TiO_2	5.87	4.28	1.71	2.18	1.55	1.40	1.40	1.43	1.60	0.93	0.94	1.49
Al_2O_3	7.09	8.75	13.75	13.36	13.43	13.44	13.61	13.22	13.74	13.24	15.92	13.61
Fe_2O_3	8.81	10.68	3.71	3.69	5.48	4.65	4.58	4.91	3.06	5.43	0.82	3.17
FeO	21.04	15.12	6.60	6.75	4.76	4.20	4.25	3.94	5.04	3.65	4.60	4.77
FeO_t	29.64	24.73	10.01	10.14	9.69	8.43	8.37	8.40	7.79	8.54	5.33	7.66
MnO	0.47	0.32	0.15	0.15	0.13	0.13	0.10	0.14	0.10	0.10	0.11	0.10
MgO	5.38	3.43	1.74	1.67	1.57	1.38	1.39	1.24	1.23	1.03	1.15	1.11
CaO	8.56	7.22	4.73	4.76	4.47	3.97	3.82	3.78	3.69	3.15	3.57	3.65
Na_2O	1.47	2.06	2.80	2.82	3.05	2.86	3.07	3.02	3.05	2.90	4.25	2.96
K_2O	0.92	1.18	4.62	4.25	3.84	4.30	4.09	3.91	4.32	4.17	4.58	4.79
P_2O_5	2.05	1.26	1.03	0.99	0.81	0.71	0.85	0.80	0.68	0.77	0.22	0.65
LOI	0.00	0.00	0.82	0.59	1.17	0.91	1.06	0.75	0.78	1.50	1.04	0.60
Total	100.97	100.65	100.41	100.46	100.66	99.42	100.68	100.07	100.32	99.80	100.62	100.58
CIPW norm												
An	8.7	9.8	10.0	9.9	10.3	9.8	10.0	9.7	9.7	9.5	9.5	8.4
Ab	12.4	17.4	23.7	23.9	25.8	24.2	26.0	25.6	25.8	24.5	36.0	25.0
Or	8.1	9.6	29.9	27.7	25.3	28.0	26.8	25.7	28.1	27.3	29.7	30.9
Qtz	0.0	4.9	10.5	12.6	14.1	15.8	16.8	18.5	17.1	18.8	9.9	16.9
Cpx	17.1	15.1	5.7	6.1	5.6	4.4	2.9	3.3	3.5	1.0	5.7	4.6
Opx	13.4	19.4	9.0	8.0	8.6	7.6	8.3	7.8	6.7	9.4	4.1	5.9
Ol	8.8	0.0	0.0	0.0	0.0	0.0	0.0	0.0	0.0	0.0	0.0	0.0
Ilm	11.2	8.1	3.3	4.1	2.9	2.7	2.7	2.7	3.0	1.8	1.8	2.8
Mag	14.0	12.0	4.8	4.9	4.7	4.1	4.1	4.1	3.8	4.1	2.6	3.7
Ap	4.8	2.9	2.4	2.3	1.9	1.7	2.0	1.9	1.6	1.8	0.5	1.5
U	1.9	3.8	1.2	0.8	1.1	1.2	1.6	1.2	0.5	1.3	1.0	0.3
Th	9.2	6.7	4.1	3.4	6.0	7.9	9.2	7.4	1.5	23.0	4.1	0.8
Pb	24	16	22	18	24	24	25	23	23	28	20	24
Zr	2817	3806	1181	1094	1167	1060	1116	1028	786	1439	702	775
Hf	68	109	28	27	29	27	30	26	19	36	18	18
Nb	140	60	39	44	32	36	46	36	33	16	30	34
Ta	7.2	2.9	2.8	1.8	1.7	2.1	3.1	2.3	1.6	0.60	1.2	1.9
Rb	14	21	124	104	117	138	152	132	139	147	108	119
Cs	0.17	0.09	0.33	0.31	0.33	0.20	0.31	0.14	0.52	0.35	0.33	0.10
Sr	99	158	276	264	305	288	384	352	284	292	281	256
Ba	77	243	1241	1227	1198	1270	1458	1293	1259	1172	1364	1251
V	236	191	49	129	65	75	72	67	76	36	30	39
Cr	32	5.5	7.4	8.4	25	4.8	17	8.8	40	14	4.1	3.6
Co	38	24	16	19	14	12	11	12	13	7.7	8.5	12
Ni	110	104	40	31	33	24	39	24	19	29	12	16
Zn	565	484	190	203	207	176	192	198	173	172	103	150
Ga	35	45	29	29	30	28	31	29	29	31	24	27
La	335	265	181	174	157	169	193	175	101	207	46	99
Ce	869	723	424	419	393	394	503	349	244	469	107	254
Pr	119	101	57	57	55	53	64	42	32	53	14	35
Nd	473	400	221	218	231	209	241	160	133	189	60	142
Sm	97	82	44	41	52	42	47	30	27	33	13	30
Eu	5.2	4.8	5.1	5.0	6.4	5.4	5.5	4.6	4.1	4.1	3.2	4.0
Gd	78	74	34	37	41	38	36	25	21	24	12	24
Tb	12	11	5.1	5.7	6.8	5.5	5.8	3.8	3.2	3.8	1.9	3.6
Dy	66	62	28	33	41	31	35	21	20	22	12	20
Ho	13	13	5.5	6.5	7.8	6	7.4	3.8	3.8	4.6	2.5	3.9
Er	36	32	15	17	20	17	21	11	10	12	6.8	11
Tm	5.1	4.5	2.2	2.4	2.6	2.4	2.9	1.5	1.4	1.7	0.9	1.5
Yb	31	27	13	14	16	15	20	10	9	11	6.6	8.9
Lu	4.1	4	1.8	2	2.2	2.1	2.9	1.4	1.3	1.7	1	1.2
Y	407	367	193	197	216	186	212	134	118	128	66	133
(La/Yb)N	7.8	7	9.6	8.7	7	8.3	6.9	13	8	13	5	8
Eu_N/Eu^*_N	0.18	0.19	0.40	0.39	0.43	0.41	0.41	0.52	0.52	0.45	0.77	0.46
Zr+Nb+Ce+Y	4233	4955	1838	1754	1808	1675	1877	1547	1181	2052	905	1196
Ga*10000/Al	9.3	9.7	4.0	4.1	4.2	3.9	4.4	4.1	4.0	4.4	2.8	3.7
T sat zr	634	835	899	890	910	913	924	916	890	970	880	885
T sat ap	800	898	1069	1068	1053	1045	1085	1081	1056	1076	910	1057

*Rb, Sr, Ni, Zn, Cu, Y, Zr, Nb by XRF, other trace elements by ICP-MS. Major elements in wt. % and trace elements in ppm.
The temperature of satiration of apatite (ap) and ziro (zr) has been calculated with the regression of Harrison & Watson (1984) and Watson and Harrison (1983), respectively.
In Eu_N/Eu^*_N, Eu^*_N is the Eu interpolated between the measured values of Sm_N and Gd_N.
Facies Gr.= granitic, Ch.= charnockitic.

Table 2 (continued)

Sample no.	98N24	AD057	98N25	AD016	AD004	MB9912	AD029	AD058	MB9916	98N60	AD011	98N19
Facies	Gr.	Gr.	Gr.	Gr.	Gr.	Gr.	Gr.	Gr.	Ch.	Ch.	Ch.	Ch.
SiO_2	63.46	63.49	64.05	64.77	65.13	66.04	67.39	69.36	63.05	63.97	64.08	65.45
TiO_2	1.12	1.48	1.36	1.20	1.16	1.04	0.69	1.20	1.55	1.21	1.12	1.12
Al_2O_3	14.39	13.24	13.63	12.91	13.01	13.66	15.20	13.24	12.32	13.46	14.19	13.26
Fe_2O_3	3.08	2.99	2.58	3.30	3.69	2.72	0.92	1.65	2.69	2.69	1.94	2.08
FeO	3.94	4.66	4.20	4.27	4.02	3.52	2.73	2.01	8.32	5.63	5.89	5.55
FeO_t	6.74	7.35	6.55	7.28	7.38	5.99	3.56	3.49	10.84	8.10	7.69	7.47
MnO	0.09	0.10	0.09	0.12	0.12	0.08	0.06	0.07	0.17	0.13	0.12	0.12
MgO	1.00	1.29	1.03	0.92	0.82	0.74	0.66	0.73	0.92	0.77	0.64	0.60
CaO	3.40	3.64	3.53	3.40	2.67	2.92	2.52	1.48	3.53	3.57	3.38	3.01
Na_2O	3.04	2.95	3.84	2.90	2.75	2.86	3.97	2.81	2.98	3.43	3.42	3.15
K_2O	5.07	4.24	4.25	4.23	4.72	4.91	5.06	6.16	3.91	3.66	4.40	4.44
P_2O_5	0.47	0.68	0.56	0.64	0.52	0.42	0.16	0.39	0.57	0.51	0.47	0.45
LOI	0.58	1.05	0.96	0.67	1.00	0.72	1.18	1.02	0.00	0.42	0.28	0.21
Total	100.11	100.33	100.58	99.85	100.10	100.04	100.85	100.34	101.04	100.13	100.64	100.11
CIPW norm												
An	9.3	9.1	6.1	8.4	7.9	8.6	7.4	4.0	7.4	9.2	9.1	7.6
Ab	25.7	25.0	32.5	24.5	23.3	24.2	33.6	23.8	25.2	29.0	28.9	26.7
Or	32.6	27.7	27.7	27.6	30.5	31.6	32.5	39.0	25.7	24.2	28.6	28.9
Qtz	15.9	19.2	15.9	21.6	21.7	21.4	17.0	24.0	19.2	19.2	17.0	20.6
Cpx	3.8	3.8	6.5	3.6	1.7	2.7	3.4	0.7	5.5	4.4	4.0	3.8
Opx	5.7	6.5	3.8	6.0	6.9	5.0	2.5	3.2	8.1	6.0	5.6	5.4
Ol	0.0	0.0	0.0	0.0	0.0	0.0	0.0	0.0	0.0	0.0	0.0	0.0
Ilm	2.1	2.8	2.6	2.3	2.2	2.0	1.3	2.3	2.9	2.3	2.1	2.1
Mag	3.3	3.6	3.2	3.5	3.6	2.9	1.7	1.7	5.2	3.9	3.7	3.6
Ap	1.1	1.6	1.3	1.5	1.2	1.0	0.4	0.9	1.3	1.2	1.1	1.0
U	0.8	0.6	0.2	0.8	1.2	0.8	0.8	0.7	0.9	1.4	0.5	0.5
Th	1.9	4.2	0.6	5.8	7.4	1.7	2.8	4.4	3.6	5.1	2.5	2.4
Pb	25	25	19	21	23	22	18	25	16	15	16	17
Zr	956	871	751	862	985	858	848	469	1122	738	653	778
Hf	24	24	18	24	27	22	19	13	27	16	17	17
Nb	22	35	28	33	32	18	21	26	43	27	24	26
Ta	1.5	1.7	1.1	0.74	1.8	0.79	0.82	1.1	2.4	1.7	1.2	1.3
Rb	128	146	110	153	160	129	124	187	115	109	114	123
Cs	0.15	0.26	0.12	0.31	0.36	0.14	0.57	0.23	0.26	0.85	0.44	0.39
Sr	297	293	292	259	283	275	240	401	200	247	282	251
Ba	1385	1196	1324	1035	1188	1255	1274	2284	865	1073	1342	1222
V	57	68	80	65	44	36	48	15	30	22	27	24
Cr	8.2	16	7.8	6.5	2.6	7.1	209	0.5	5.0	3.9	1.1	4.4
Co	11	12	15	12	8.3	7.8	25	4.7	11	8.0	9.1	8.3
Ni	19	23	14	20	30	17	2.6	3.6	30	13	10	15
Zn	141	154	148	172	187	135	65	64	211	169	147	157
Ga	29	28	27	29	32	29	21	23	29	29	28	27
La	101	122	90	131	123	79	38	59	87	49	51	53
Ce	251	289	211	296	287	190	73	110	212	120	120	116
Pr	35	37	28	40	40	26	10	12	30	18	17	15
Nd	138	149	106	150	158	107	38	43	129	76	68	64
Sm	28	31	20	29	32	22	7.1	7.6	29	17	15	14
Eu	4.3	4.2	3.8	4.3	4.2	3.9	2.5	1.6	3.7	4.2	4.8	4.2
Gd	25	24	19	27	29	18	6.2	6.5	25	16	15	13
Tb	3.7	3.8	2.8	4.1	4.4	2.8	0.9	0.9	4.1	2.6	2.3	2.0
Dy	21	23	16	24	26	16	6.2	5.4	22	15	13	11
Ho	4.1	4.9	3.1	5	5.3	3.1	1.3	1.1	4.4	2.9	2.8	2.2
Er	11	12	8.3	14	14	7.8	3.9	3.1	12	8.1	7.4	6.1
Tm	1.5	1.6	1.2	1.9	2	1	0.6	0.4	1.6	1.2	1.0	0.90
Yb	9	11	7.1	12	12	6.4	3.9	2.9	10	7.7	6.3	5.7
Lu	1.2	1.5	1	1.6	1.6	0.9	0.7	0.4	1.5	1.1	0.90	0.80
Y	123	138	95	153	156	93	41	34	145	97	78	76
(La/Yb)N	8	8	9	8.1	7.7	8.8	6.9	15	6	4.6	5.8	6.6
Eu_N/Eu^*_N	0.50	0.47	0.60	0.47	0.43	0.59	1.1	0.69	0.42	0.78	0.96	0.97
Zr+Nb+Ce+Y	1352	1332	1085	1344	1460	1159	984	639	1522	982	875	996
Ga*10000/Al	3.8	4.0	3.7	4.2	4.6	4.0	2.6	3.3	4.4	4.1	3.7	3.8
T sat zr	918	901	876	906	935	919	922	871	919	887	877	900
T sat ap	1014	1067	1045	1072	1046	1027	924	1051	1037	1031	1021	1030

*Rb, Sr, Ni, Zn, Cu, Y, Zr, Nb by XRF, other trace elements by ICP-MS. Major elements in wt. % and trace elements in ppm.
The temperature of satiration of apatite (ap) and ziro (zr) has been calculated with the regression of Harrison & Watson (1984) and Watson and Harrison (1983), respectively.
In Eu_N/Eu^*_N, Eu^*_N is the Eu interpolated between the measured values of Sm_N and Gd_N.
Facies Gr.= granitic, Ch.= charnockitic.

Table 2 (continued)

Sample no.	AD034	AD002	AD015	AD003	AD012	98N26	AD035	98N28	AD014	AD009	98N58	AD005
Facies	Ch.	Ch.	Ch.	Ch.	Ch.	Ch.	Ch.	Ch.	Ch.	Ch.	Ch.	Ch.
SiO_2	65.51	65.78	66.04	66.05	66.17	66.18	66.46	66.51	66.80	66.88	67.15	67.22
TiO_2	1.08	1.10	1.05	1.02	1.00	1.11	1.11	1.06	1.02	0.92	1.06	1.01
Al_2O_3	13.86	13.22	13.06	13.08	13.50	12.82	13.43	13.08	13.16	13.00	13.53	13.23
Fe_2O_3	1.98	1.76	2.28	1.81	1.59	3.82	1.88	1.71	1.94	2.46	1.66	1.55
FeO	5.46	5.69	5.17	5.14	5.14	3.59	5.55	5.49	5.00	4.76	5.03	4.97
FeO_t	7.24	7.32	7.27	6.81	6.61	7.06	7.24	7.07	6.79	7.01	6.56	6.40
MnO	0.12	0.13	0.12	0.11	0.11	0.10	0.12	0.12	0.11	0.11	0.13	0.11
MgO	0.69	0.65	0.58	0.58	0.57	0.65	0.61	0.58	0.51	0.52	0.66	0.52
CaO	3.35	3.26	2.80	2.81	3.03	2.91	2.84	2.97	2.76	2.67	3.02	2.76
Na_2O	3.50	3.20	3.13	3.62	3.16	2.88	3.32	3.07	3.14	3.47	3.12	3.04
K_2O	4.10	4.08	4.24	4.19	4.46	4.40	4.56	4.37	4.51	4.53	4.03	4.66
P_2O_5	0.41	0.46	0.41	0.40	0.41	0.43	0.40	0.43	0.41	0.37	0.44	0.39
LOI	0.82	0.19	0.64	0.33	0.27	1.08	0.30	0.39	0.25	0.76	0.36	0.16
Total	101.48	100.20	100.15	99.76	100.02	100.40	101.19	100.43	100.21	101.02	100.79	100.21
CIPW norm												
An	8.7	8.4	7.8	5.8	8.2	7.8	7.0	7.7	7.2	5.2	9.7	7.4
Ab	29.6	27.1	26.5	30.6	26.7	24.4	28.1	26.0	26.6	29.4	26.4	25.7
Or	26.8	26.7	27.7	27.4	29.0	28.6	29.6	28.4	29.3	29.4	26.4	30.2
Qtz	19.2	21.6	22.3	20.3	21.4	23.3	20.5	22.6	22.5	20.8	23.9	23.0
Cpx	4.5	4.2	3.0	4.8	3.6	3.3	3.9	3.7	3.3	4.9	2.1	3.3
Opx	5.2	5.3	5.7	4.3	4.8	5.4	5.2	5.1	4.9	4.5	5.7	4.6
Ol	0.0	0.0	0.0	0.0	0.0	0.0	0.0	0.0	0.0	0.0	0.0	0.0
Ilm	2.1	2.1	2.0	1.9	1.9	2.1	2.1	2.0	1.9	1.8	2.0	1.9
Mag	3.5	3.5	3.5	3.3	3.2	3.4	3.5	3.4	3.3	3.4	3.2	3.1
Ap	1.0	1.1	1.0	0.9	1.0	1.0	0.9	1.0	1.0	0.9	1.0	0.9
U	0.2	0.6	0.8	0.6	0.3	0.6	0.48	0.29	0.62	0.70	0.87	0.40
Th	0.7	2.4	3.5	1.8	1.9	2.4	2.9	1.6	3.5	2.6	3.6	4.4
Pb	15	16	17	21	15	21	19	16	15	18	17	19
Zr	628	648	772	768	645	925	772	687	665	714	573	687
Hf	15	16	18	26	15	25	21	16	18	18	14	20
Nb	21	23	26	23	21	25	29	24	23	27	42	26
Ta	1.1	1.3	2.3	3.2	1.4	0.58	1.7	1.3	0.71	2.3	4.9	1.2
Rb	94	105	124	108	114	132	121	120	118	133	115	134
Cs	0.77	0.51	0.27	0.24	0.32	0.15	0.75	0.14	0.42	0.54	0.55	0.30
Sr	273	273	212	221	258	254	191	241	205	215	249	219
Ba	1357	1242	983	1073	1235	1106	1020	1194	1098	1042	1138	1127
V	20	22	11	19	29	49	19	22	30	11	26	20
Cr	1.3	1.6	1.2	0.30	2.0	3.2	-	4.4	1.9	1.4	4.4	0.20
Co	9.3	7.2	7.7	6.2	8.8	10	7.7	7.3	9.7	7.0	7.2	6.2
Ni	5.8	11	14	5.1	14	22	17	7.4	11	7.3	8.3	14
Zn	132	144	164	138	133	161	149	144	138	142	150	131
Ga	27	30	27	27	27	29	26	27	24	27	28	26
La	44	53	58	31	43	100	68	50	62	61	55	67
Ce	106	109	132	74	103	241	170	113	141	137	123	153
Pr	14	15	18	10	13	34	23	15	19	19	17	21
Nd	64	66	78	46	59	139	102	68	76	80	69	83
Sm	15	14	16	10	13	29	23	16	17	18	15	18
Eu	4.8	4.7	3.6	4.0	4.3	3.3	4.1	4.0	3.8	3.5	4.2	4.1
Gd	13	15	16	9.7	14	27	21	14	16	16	13	18
Tb	2.2	2.3	2.4	1.5	1.9	4.0	3.3	2.2	2.5	2.5	2.0	2.7
Dy	13	13	14	8.3	11	24	20	12	14	14	11	16
Ho	2.6	2.7	2.6	1.7	2.4	4.6	4.2	2.4	2.8	2.7	2.3	3.2
Er	6.9	7.0	7.3	4.5	6.1	12	10	6.7	7.5	7.3	6.3	8.6
Tm	0.90	1.0	1.1	0.60	0.90	1.7	1.3	1.0	1.1	1.0	0.90	1.3
Yb	6.1	6.2	7.0	3.8	5.6	9.5	8.7	5.9	6.5	6.5	5.7	7.5
Lu	0.90	0.90	1.0	0.50	0.80	1.3	1.2	0.90	0.90	1.0	0.80	1.2
Y	70	78	90	47	71	137	100	78	81	94	76	89
(La/Yb)N	5.2	6.1	5.9	5.8	5.5	7.6	5.6	6.1	6.8	6.7	6.9	6.4
Eu_N/Eu^*_N	1.1	0.99	0.69	1.2	1.0	0.36	0.56	0.82	0.70	0.62	0.94	0.70
Zr+Nb+Ce+Y	825	857	1020	912	841	1328	1071	902	910	972	814	955
Ga*10000/Al	3.7	4.2	3.9	3.9	3.8	4.3	3.7	3.9	3.4	3.9	3.9	3.7
T sat zr	875	880	906	897	884	924	901	890	890	890	880	895
T sat ap	1018	1036	1023	1020	1025	1031	1025	1035	1031	1019	1044	1029

*Rb, Sr, Ni, Zn, Cu, Y, Zr, Nb by XRF, other trace elements by ICP-MS. Major elements in wt. % and trace elements in ppm.
The temperature of satiration of apatite (ap) and ziro (zr) has been calculated with the regression of Harrison & Watson (1984) and Watson and Harrison (1983), respectively.
In Eu_N/Eu^*_N, Eu^*_N is the Eu interpolated between the measured values of Sm_N and Gd_N.
Facies Gr.= granitic, Ch.= charnockitic.

Table 2 (continued)

Sample no.	MB9925	AD006	AD017	AD040	AD037	AD026	AD023	AD001	MB9935	AD010	98N59
Facies	Ch.	Ch.	Ch.	Ch.	Ch.	Ch.	Ch.	Ch.	Ch.	Ch.	Ch.
SiO_2	67.44	67.91	67.93	68.45	68.87	69.39	69.94	70.59	71.05	71.83	71.91
TiO_2	0.96	0.85	1.04	0.93	0.85	0.86	0.77	0.66	0.33	0.58	0.20
Al_2O_3	12.88	13.07	11.97	13.26	13.04	13.08	13.20	12.88	13.82	12.35	13.38
Fe_2O_3	1.89	1.85	2.03	1.58	1.23	4.00	2.02	2.80	1.00	2.54	0.94
FeO	5.17	4.51	5.35	4.63	4.79	1.58	3.45	2.37	1.82	2.36	1.44
FeO_t	6.91	6.20	7.22	6.05	5.90	5.18	5.27	4.90	2.72	4.66	2.29
MnO	0.11	0.10	0.12	0.10	0.11	0.07	0.07	0.05	0.06	0.05	0.04
MgO	0.51	0.47	0.56	0.49	0.54	0.41	0.35	0.23	0.25	0.20	0.32
CaO	2.75	2.47	2.50	2.52	2.50	1.87	1.98	1.66	1.71	1.24	1.39
Na_2O	3.04	3.10	2.70	3.27	3.22	3.00	3.05	2.73	3.00	2.32	2.52
K_2O	4.56	4.74	4.59	4.62	4.65	5.37	5.16	5.20	5.95	6.12	6.72
P_2O_5	0.38	0.34	0.33	0.34	0.34	0.26	0.26	0.22	0.10	0.11	0.07
LOI	0.31	0.50	0.34	0.29	0.26	0.97	0.62	0.70	0.60	0.86	0.98
Total	100.62	100.44	100.10	100.99	100.93	101.03	101.25	100.36	99.89	100.84	100.07
CIPW norm											
An	6.7	6.4	5.7	6.6	6.1	5.1	5.8	6.2	5.4	3.9	4.0
Ab	25.7	26.2	22.8	27.7	27.2	25.4	25.8	23.1	25.4	19.6	21.3
Or	29.6	30.6	29.7	29.9	30.1	34.4	33.1	33.3	37.8	38.8	42.3
Qtz	23.5	23.5	26.1	23.5	24.2	24.6	25.3	28.2	24.9	29.2	26.2
Cpx	3.8	3.1	4.0	3.2	3.5	2.2	2.0	0.5	2.1	1.3	2.0
Opx	4.8	4.6	5.1	4.3	4.3	3.8	4.0	4.3	1.8	3.6	1.8
Ol	0.0	0.0	0.0	0.0	0.0	0.0	0.0	0.0	0.0	0.0	0.0
Ilm	1.8	1.6	2.0	1.8	1.6	1.6	1.5	1.3	0.6	1.1	0.4
Mag	3.3	3.0	3.5	2.9	2.9	2.5	2.6	2.4	1.3	2.3	1.1
Ap	0.9	0.8	0.8	0.8	0.8	0.6	0.6	0.5	0.2	0.3	0.2
U	0.6	2.5	0.33	0.36	0.7	0.5	0.57	0.34	0.2	0.52	6.3
Th	3.2	10.8	1.2	3.9	4.9	4.6	3.3	0.78	1.2	0.85	37.8
Pb	18	22	14	18	23	21	18	22	22	17	27
Zr	643	609	744	672	670	673	577	886	284	340	230
Hf	18	18	19	17	19	18	19	23	8	9.4	8.0
Nb	26	26	28	25	38	34	18	10	10	8.0	7.9
Ta	1.4	1.7	0.68	1.5	2.0	1.7	0.8	1.0	0.64	1.3	1.3
Rb	138	157	128	127	131	148	126	128	191	176	181
Cs	0.27	0.62	0.15	0.73	0.47	1.53	0.14	0.12	0.57	0.76	0.69
Sr	209	191	202	190	181	170	161	109	262	203	191
Ba	1055	1022	1097	1000	1019	925	977	755	1582	1413	1089
V	21	21	30	12	5	11	16	10	16	14	16
Cr	4.6	2.1	3.4	7.5	19	159	-	-	4.6	-	-
Co	6.8	6.9	9.0	5.2	6.6	27	0.65	3.5	4.1	4.1	2.5
Ni	13	14	13	9.8	7.8	8.7	4.2	5.4	-	1.0	-
Zn	130	126	134	119	127	110	100	111	74	101	40
Ga	28	26	25	25	25	25	24	32	24	21	17
La	61	66	45	60	76	70	58	37	35	19	48
Ce	140	154	110	144	187	184	145	85	65	44	106
Pr	19	21	15	19	26	25	22	11	8.6	6	13
Nd	77	80	65	82	113	108	97	46	35	27	50
Sm	18	17	13	18	25	25	23	10	7.3	6.4	9.9
Eu	3.7	3.7	3.6	3.8	4.3	3.1	3.2	3.2	4.2	3.8	2.5
Gd	17	17	14	16	21	22	22	9.3	7.2	7.1	8.4
Tb	2.5	2.6	2.1	2.6	3.6	3.7	3.2	1.4	1.2	1.1	1.3
Dy	14	15	13	16	21	22	20	7.4	6.6	6.6	7.0
Ho	2.8	3.1	2.5	3.2	4.3	4.4	4.0	1.5	1.3	1.4	1.4
Er	7.5	8.4	6.5	8.4	11	12	9.8	3.7	3.6	3.8	3.7
Tm	1.1	1.2	1.0	1.1	1.5	1.6	1.2	0.50	0.6	0.60	0.50
Yb	6.8	7.6	5.9	7.4	9.6	9.8	7.3	3.1	3.8	3.5	3.6
Lu	1	1.1	0.90	1.0	1.4	1.3	1.1	0.40	0.6	0.50	0.50
Y	90	88	78	85	106	120	100	40	39	39	41
(La/Yb)N	6.5	6.2	5.5	5.8	5.7	5.1	5.7	8.5	6.7	3.8	9.7
Eu_N/Eu^*_N	0.65	0.68	0.81	0.69	0.57	0.40	0.43	1.0	1.8	1.7	0.85
Zr+Nb+Ce+Y	899	876	959	926	1000	1011	841	1021	398	431	384
Ga*10000/Al	4.1	3.8	3.9	3.6	3.6	3.6	3.4	4.7	3.3	3.2	2.3
T sat zr	885	886	903	895	894	905	890	948	826	847	809
T sat ap	1028	1019	1015	1024	1028	1000	1006	993	912	929	886

*Rb, Sr, Ni, Zn, Cu, Y, Zr, Nb by XRF, other trace elements by ICP-MS. Major elements in wt. % and trace elements in ppm.
The temperature of satiration of apatite (ap) and ziro (zr) has been calculated with the regression of Harrison & Watson (1984) and Watson and Harrison (1983), respectively.
In Eu_N/Eu^*_N, Eu^*_N is the Eu interpolated between the measured values of Sm_N and Gd_N.
Facies Gr.= granitic, Ch.= charnockitic.

Table 3: TIMS U-Pb geochronological data on zircon

Type (1)	# (2)	Weight (µg)	U (ppm)	Pb rad (ppm)	$^{206}Pb/^{204}Pb$ (3)	$^{208}Pb/^{206}Pb$ (3)	$^{206}Pb/^{238}U$ (4)	$^{207}Pb/^{235}U$ (4)	$^{207}Pb/^{206}Pb$ (4)	$^{206}Pb/^{238}U$	$^{207}Pb/^{235}U$	$^{207}Pb/^{206}Pb$
AD017 - Charnockitic facies												
c.p.	6	108	110	18	10469	0.1588	0.1546 (0.17%)	1.494 (0.19%)	0.0701 (0.07%)	927	928	931
l.p.	4	64	55	9	2185	0.1648	0.1494 (0.39%)	1.442 (0.58%)	0.0700 (0.42%)	898	907	929
l.p.	5	64	122	19	7085	0.1568	0.1475 (0.17%)	1.424 (0.20%)	0.0700 (0.10%)	887	899	929
AD060 - Granitic facies												
l.p.	6	78	140	23	3383	0.1472	0.1544 (0.21%)	1.488 (0.27%)	0.0699 (0.16%)	925	926	926
c.p.	5	55	350	57	4710	0.1575	0.1535 (0.62%)	1.479 (0.63%)	0.0699 (0.12%)	920	922	925
l.p.	6	38	143	23	4129	0.1488	0.1533 (0.24%)	1.479 (0.36%)	0.0699 (0.26%)	920	922	926

(1) Type of crystals: c.p., short and prismatic; l.p., long and prismatic.
(2) Number of analysed crystals.
(3) Measured isotopic ratios.
(4) Calculated isotopic ratios. 2σ errors within brackets.
Common Pb of each fraction was estimated with the two stage model of Stacey & Kramers (1975).

Table 4: Whole-rock Rb-Sr and Sm-Nd isotopic data

Sample	Rb	Sr	$^{87}Rb/^{86}Sr$	$^{87}Sr/^{86}Sr$	2 s.e.	$^{87}Sr/^{86}Sr_{930}$	Sm	Nd	$^{147}Sm/^{144}Nd$	$^{143}Nd/^{144}Nd$	2 s.e.	$(^{143}Nd/^{144}Nd_{930})$*	(ε_{Nd930})**
AD060	117	305	1.11	0.721571	16	0.70680	49.0	232	0.1280	0.512162	7	0.51138	-1.1
AD061	152	384	1.15	0.720686	11	0.70544	42.4	233	0.1100	0.512050	8	0.51138	-1.2
AD016	153	259	1.71	0.730564	8	0.70779	29.5	142	0.1261	0.512105	9	0.51134	-2.0
MB9913	14.3	99	0.42	0.71124	10	0.70568	76.5	376	0.1230	0.512117	13	0.51137	-1.4
98N21	104	264	1.14	0.721869	15	0.70670	42.8	218	0.1186	0.512113	8	0.51139	-0.9
MB9912	129	275	1.36	0.725624	24	0.70755	22.5	111	0.1225	0.512121	12	0.51137	-1.3
MB9916	115	200	1.67	0.733292	19	0.71112	28.8	131	0.1332	0.512232	9	0.51142	-0.4
AD035	121	191	1.84	0.734454	9	0.71002	21.7	97.5	0.1346	0.512315	12	0.51149	1.1
AD017	128	202	1.84	0.735526	19	0.71109	15.2	67.6	0.1360	0.512271	7	0.51144	0.1
AD023	126	161	2.27	0.739879	12	0.70968	22.0	95.4	0.1395	0.512319	14	0.51147	0.6
98N59	181	191	2.76	0.757885	12	0.72126	9.40	46.8	0.1215	0.512102	9	0.51136	-1.5
98N19	123	251	1.42	0.730042	12	0.71115	13.8	64.6	0.1292	0.512219	7	0.51143	-0.1
AD040	127	190	1.94	0.736117	13	0.71034	18.0	82.6	0.1318	0.512235	8	0.51143	-0.1
AD005	134	219	1.77	0.734381	10	0.71079	17.0	77.5	0.1326	0.512237	9	0.51143	-0.2
MB9925	138	209	1.92	0.73669	19	0.71122	17.5	80.1	0.1321	0.512254	11	0.51145	0.2
MB9935	191	262	2.12	0.739557	17	0.71143	6.70	31.7	0.1278	0.512236	12	0.51146	0.4

* $\lambda\ ^{147}Sm = 6.54 \times 10^{-12}\ y^{-1}$ (Steiger and Jäger, 1977).

** Present-day $(^{147}Sm/^{144}Nd)_{CHUR}$ and $(^{143}Nd/^{144}Nd)_{CHUR}$ = 0.1966 and 0.512638, respectively (Jacobsen & Wasserburg et al., 1980).

Rb, Sr, Sm, Nd are given in ppm.

Table 5: Isotopic composition of Pb in the Farsund samples

Sample	$^{206}Pb/^{204}Pb$	$^{207}Pb/^{204}Pb$	$^{208}Pb/^{204}Pb$	Pb	U	Th	$^{238}U/^{204}Pb$	$^{235}U/^{204}Pb$	$^{232}Th/^{204}Pb$	$^{206}Pb/^{204}Pb$*	$^{207}Pb/^{204}Pb$*	$^{208}Pb/^{204}Pb$*
AD060	17.5991	15.5200	37.5252	24	1.1	6	2.84	0.021	16.0	17.16	15.49	36.77
AD061	17.8598	15.5421	38.0039	25	1.6	9.2	4.00	0.029	23.8	17.24	15.50	36.88
AD016	17.7402	15.5395	37.7907	21.4	0.79	5.8	2.30	0.017	17.4	17.38	15.51	36.97
98N21	17.6185	15.5245	37.3640	17.5	0.78	3.4	2.75	0.020	12.4	17.19	15.49	36.78
MB9912	17.5543	15.5222	37.0054	22.5	0.77	1.7	2.10	0.015	4.8	17.23	15.50	36.78
MB9916	18.0759	15.5727	37.8476	16.1	0.87	3.6	3.39	0.025	14.5	17.55	15.54	37.17
AD035	17.9458	15.5663	37.7524	19.2	0.48	2.9	1.56	0.011	9.7	17.70	15.55	37.29
AD017	17.9102	15.5635	37.4943	14	0.33	1.2	1.47	0.011	5.5	17.68	15.55	37.23
AD023	17.9711	15.566	37.735	17.7	0.57	3.3	2.01	0.015	12.0	17.66	15.54	37.17
MB9925	18.0132	15.5716	37.7853	18.1	0.57	3.2	1.97	0.014	11.4	17.71	15.55	37.25
MB9935	17.8751	15.5588	37.4029	21.8	0.23	1.2	0.66	0.005	3.5	17.77	15.55	37.24

*$\lambda^{238}U=1.55125x10^{-10}y^{-1}$,$\lambda^{235}U = 9.8485x10^{-10}y^{-1}$, $\lambda^{232}Th = 4.9475 \times 10^{-11}$ y^{-1} (Steiger and Jäger, 1977). *Initial ratios calculated at 930 Ma.
Pb, U, Th are given in ppm. Samples AD060, AD061, AD016, 98N21, MB9912 belong to the granitic facies, the others, to the charnockitic facies.

Table 6: Least square regression models

Crystallization in the charnockitic facies

	Lyngdal	L_0	L_1	Bulk Cumulate	Mineral compositions*					
	98N06	**AD011**	**AD23**	Cumulate	Plag	Opx	Cpx	Mag	Ilm	Ap
SiO_2	65.2	64.40	69.9	50.12	61.91	51.43	50.60	0.00	0.00	0.00
TiO_2	1.11	1.13	0.77	2.22	0.00	0.71	0.55	0.70	51.56	0.00
Al_2O_3	14.4	14.26	13.2	17.48	23.07	2.71	2.33	0.59	0.00	0.00
FeO_{tot}	5.8	7.73	5.27	15.16	0.96	28.32	15.26	98.71	47.47	0.33
MnO	0.1	0.12	0.07	0.08	0.00	0.53	0.49	0.00	0.97	0.02
MgO	1.39	0.64	0.35	0.77	0.00	10.29	9.97	0.00	0.00	0.05
CaO	3.51	3.40	1.98	7.64	7.06	5.54	20.26	0.00	0.00	56.25
Na_2O	3.28	3.44	3.05	4.20	5.57	0.47	0.54	0.00	0.00	0.04
K_2O	4.32	4.42	5.16	1.07	1.43	0.00	0.00	0.00	0.00	0.01
P_2O_5	0.39	0.47	0.26	1.12	0.00	0.00	0.00	0.00	0.00	43.30

* Mineral compositions are from experimental data of Bogaerts et al. (2006) (Plag#50-27, Opx#06-22, Cpx#06-25, Bt#06-11, Amp#06-29) except for magnetite, ilmenite and apatite for which natural compositions have been used. Sample 98N06 is one of the staring compositions used by Bogaerts et al. (2006). Plag=plagioclase, Opx=orthopyroxene, Cpx=clinopyroxene, Mag=magnetite, Ilm=ilmenite, Ap=apatite. L_0 designates the sample selected as the starting composition, L_1, the sample selected as representative of the residual liquid. See text for explanation.

Composition of the bulk cumulate
C = 74.65% Plag +4.11% Opx+3.44% Cpx + 10.96% Mag +4.07% Ilm +2.58 % Ap+0.17% Zr
F = 0.7410
$\Sigma r^2 = 0.1644$

Crystallization in the granitic facies

	Lyngdal	L_0	L_1	Bulk Cumulate	Mineral compositions*					
	98N50	**AD60**	**AD004**	Cumulate	Plag	Amp	Bt	Ap	Mag	Ilm
SiO_2	60.2	60.8	66.27	44.38	59.8	42.3	40.3	0	0	0
TiO_2	1.74	1.58	1.18	2.77	0	2.27	3.71	0	13.1	47.3
Al_2O_3	13.8	13.7	13.24	15.06	25.2	10.1	12.7	0	2.43	0.34
FeO_{tot}	9.26	9.85	7.51	16.78	0.16	23.1	18.2	0.33	82.9	49.9
MnO	0.16	0.13	0.12	0.15	0	0.25	0.33	0.02	0.31	0.35
MgO	2.15	1.60	0.83	3.86	0.02	7.11	14.5	0.05	1.28	2.20
CaO	5.35	4.54	2.72	9.98	6.84	11.2	0	56.3	0	0
Na_2O	3.15	3.10	2.80	3.92	7.65	1.99	0.11	0.04	0	0
K_2O	2.88	3.90	4.80	1.25	0.36	1.77	10.1	0.01	0	0
P_2O_5	0.85	0.81	0.53	1.61	0	0	0	43.3	0	0

* Mineral compositions are from experimental data of Bogaerts et al. (2006) except for apatite for which a natural composition has been used. Sample 98N50 is one of the starting compositions used by Bogaerts et al. (2006).

Composition of the bulk cumulate
C = 39.05% Plag +46.78% Amp + 2.83% Bt + 5.38% Mag +1.91% Ilm +3.71 % Ap+0.34% Zr

F = 0.7499
$\Sigma r^2 = 0.0008$

Table 7: Partition coefficients used for trace elements

	plagioclase	orthopyroxene	clinopyroxene	amphibole	biotite	apatite	magnetite	ilmenite	zircon
Rb	0.3[a]	0.062[b]	0.03[a]	0.18[b]	1.35[i]	0.01[a]	0.01[a]	0.01[a]	0.001
Sr	4[a]	0.068[b]	0.5[a]	0.01[a]	0.31[a]	2[a]	0.01[a]	0.01[a]	0.001
Ba	1.8[b]	0.07[b]	0.1[a]	0.62[g]	13.9[b]	0.01[a]	0.1[a]	0.01[a]	0.001
Ce	0.2[a]	0.082[c]	0.075[e]	0.53[a]	0.32[a]	21.1[k]	0.71[a]	0.0019[n]	0.36[p]
Sm	0.1[a]	0.133[c]	0.22[e]	2[a]	0.26[a]	46[k]	1.2[a]	0.0023[n]	0.8[p]
Eu	2[a]	0.113[c]	0.2[e]	1.9[a]	0.24[a]	25.5[k]	0.91[a]	0.0009[n]	1.22[p]
Tb	0.1[a]	0.215[c]	0.258[e]	2[a]	0.28[a]	39.4[k]	1.3[a]	0.0095[n]	20.7[p]
Yb	0.1[a]	0.73[c]	0.3[e]	2.1[a]	0.44[a]	15.4[k]	0.44[a]	0.057[n]	277[p]
V	0.2[a]	6[d]	18[f]	4.92[h]	0.0001	0[a]	2[l]	14[l]	0.001
Co	0.1[a]	38[a]	17[a]	6.1[a]	4[i]	0.01[a]	32[m]	13[o]	0.001
Zn	0.4[a]	3.7[a]	2[a]	1.6[a]	11.4[j]	0.01[a]	15[a]	10[a]	0.001

[a] Bacon & Druitt (1988); [b] Ewart & Griffin (1994); [c] Nagasawa & Schnetzler (1971); [d] Sisson (1991); [e] McKay (1989); [f] Reid (1983); [g] Nagasawa (1973); [h] Sisson (1994); [i] Villemant (1988); [j] Bea et al (1994); [k] Fujimaki (1986); [l] Toplis & Corgne (2002); [m] Streck & Grunder (1997); [n] Nakamura et al (1986); [o] Mahood & Hildreth (1983); [p] Sano et al (2002).

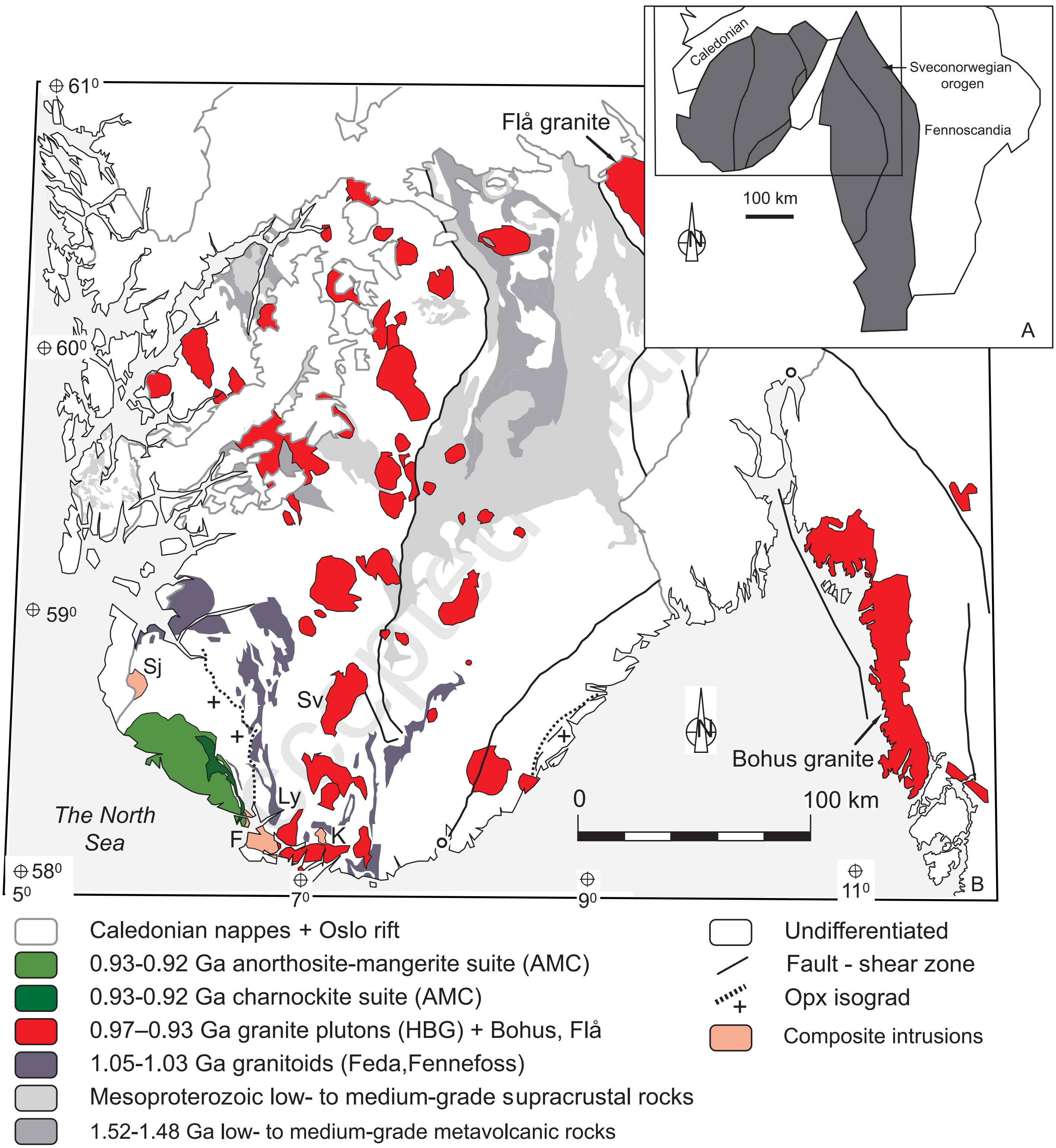

Fig. 1 - Vander Auwera et al.

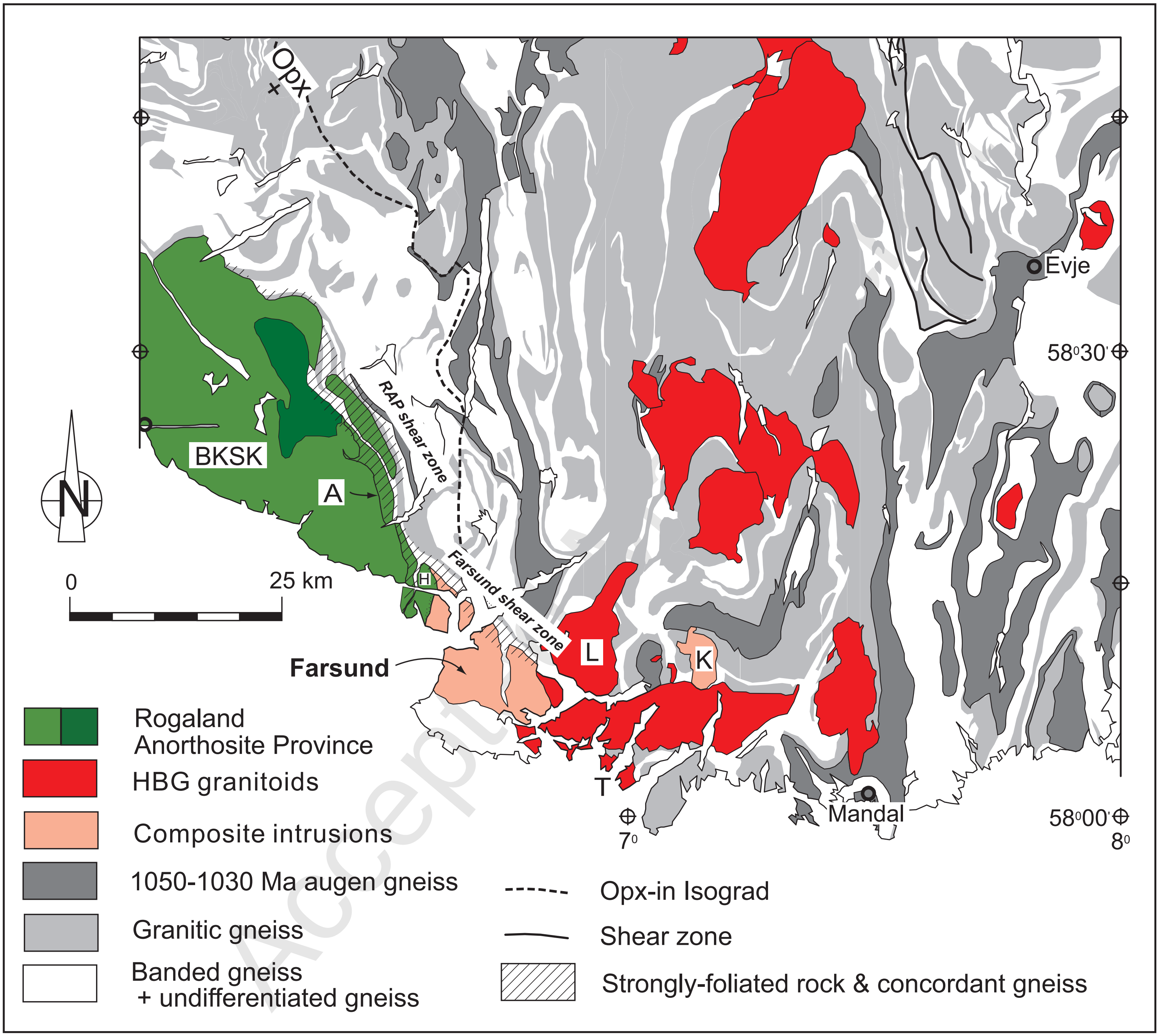

Fig. 2 - Vander Auwera et al.

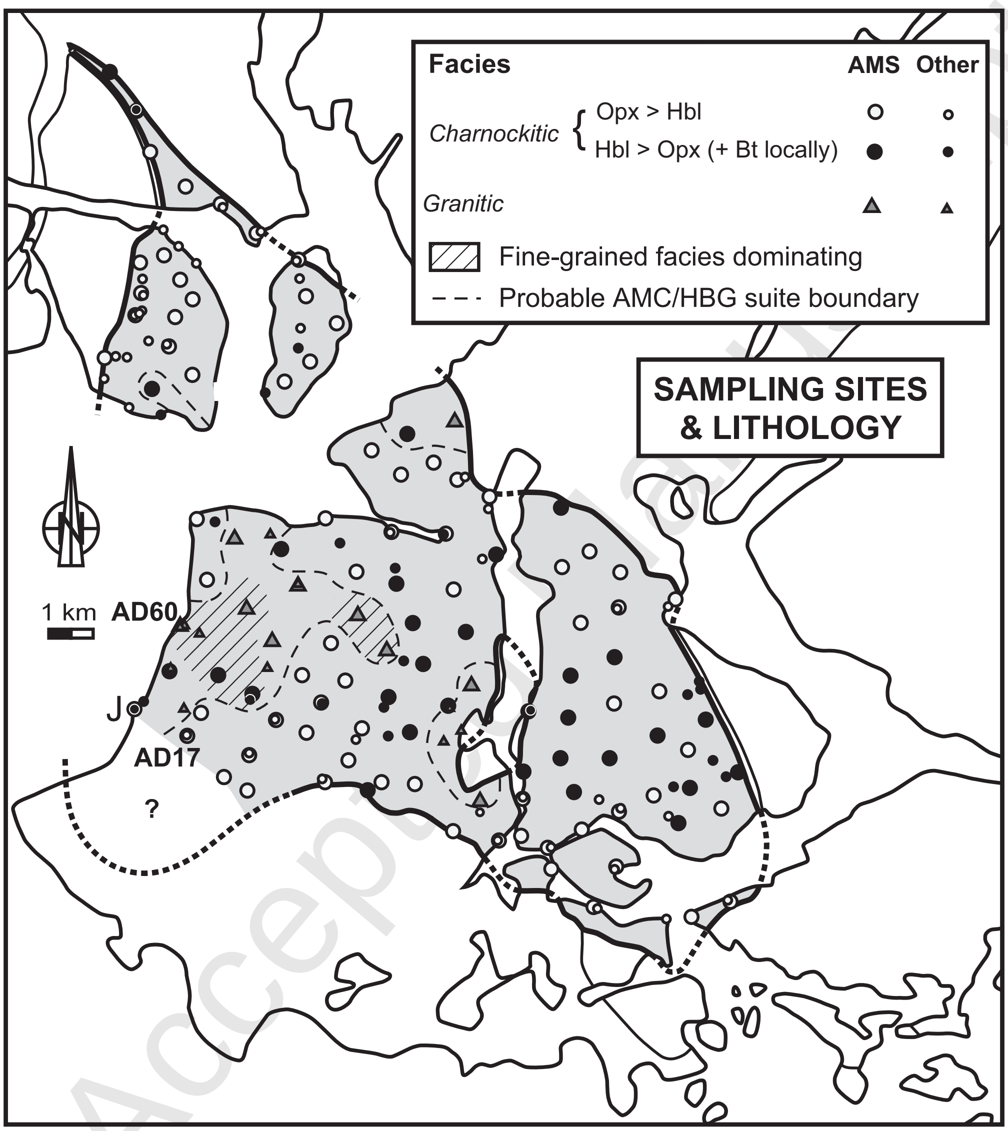

Fig. 3 - Vander Auwera et al.

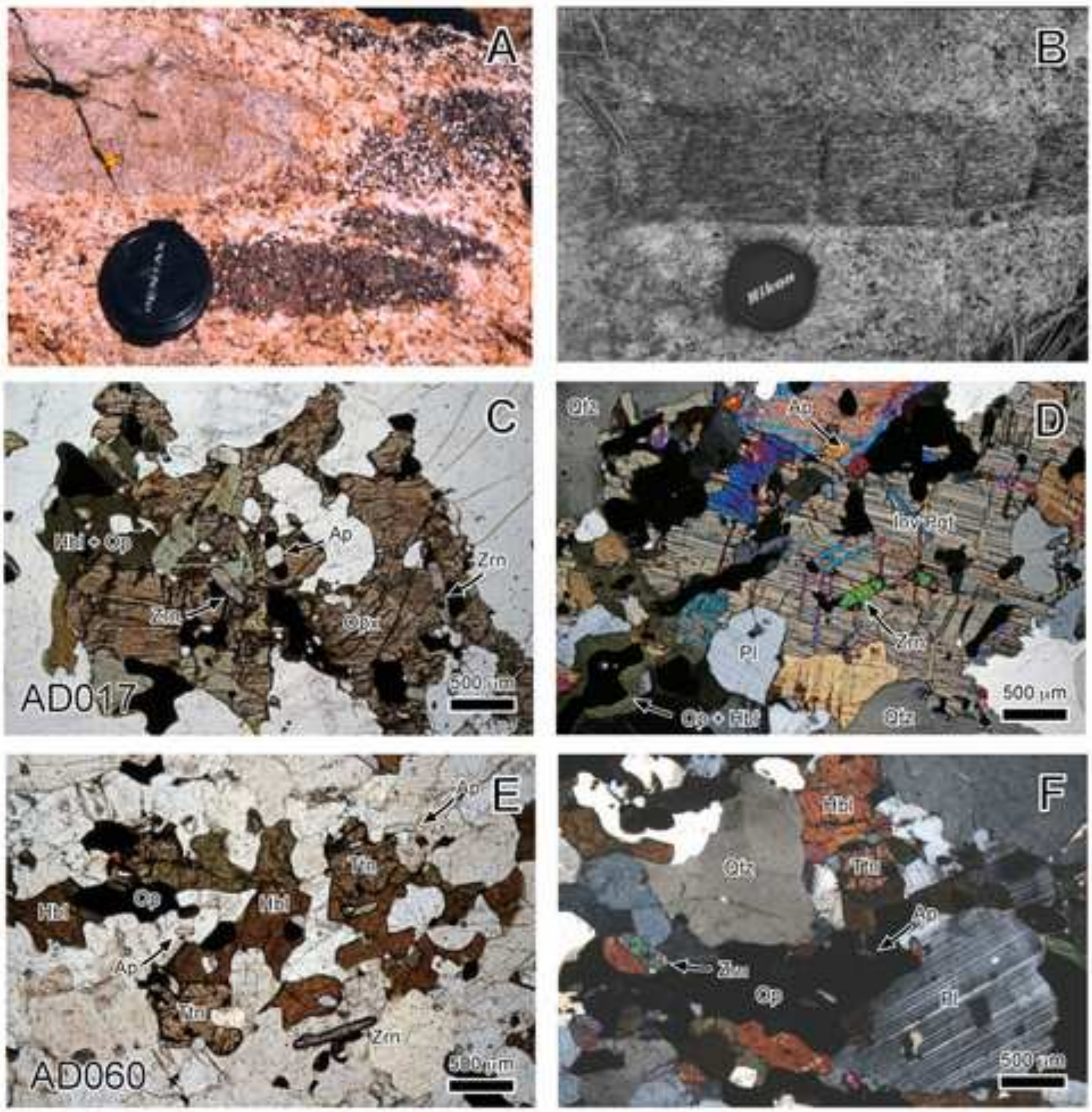

Fig. 4 - Vander Auwera et al.

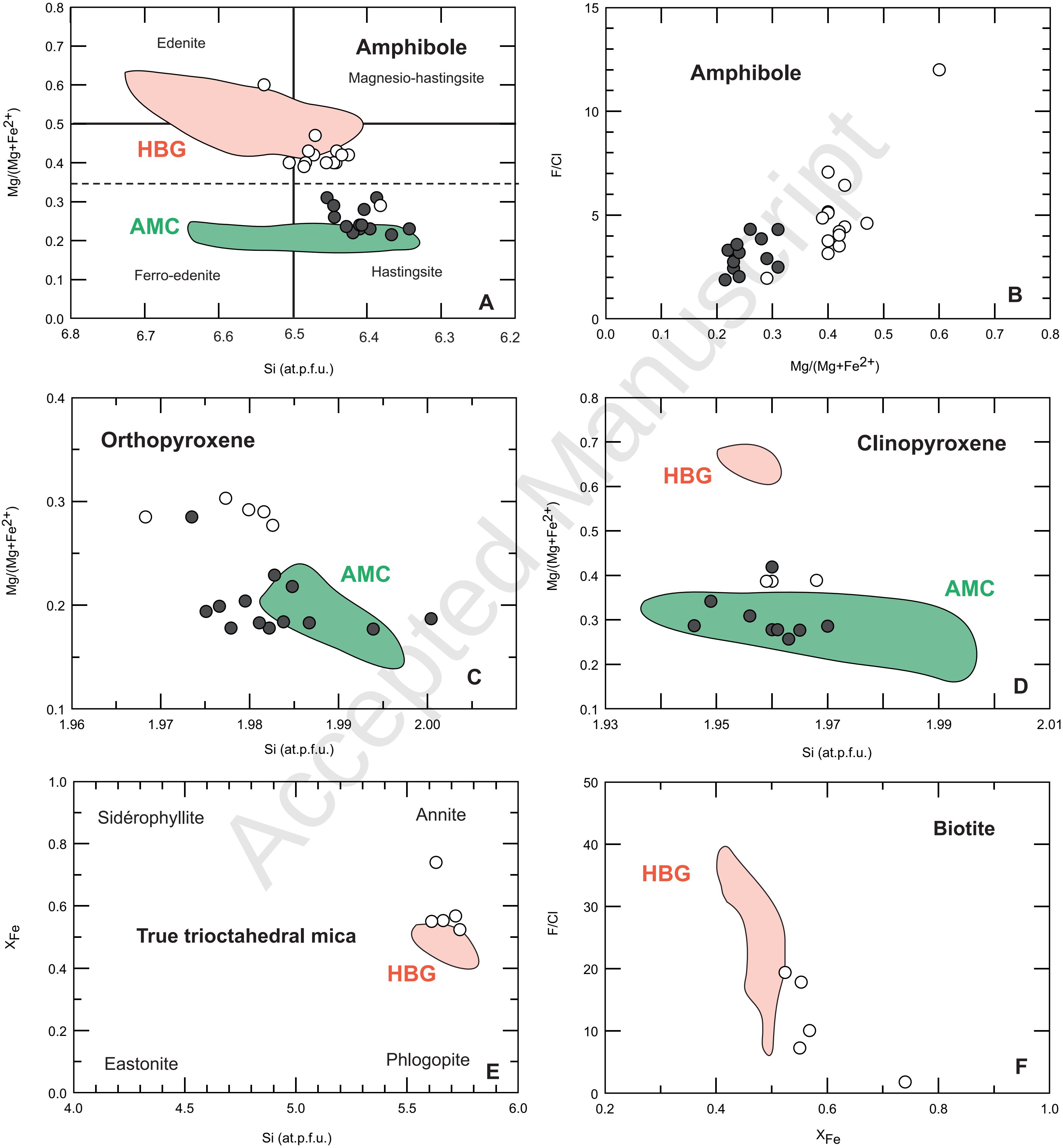

Fig. 5 - Vander Auwera et al.

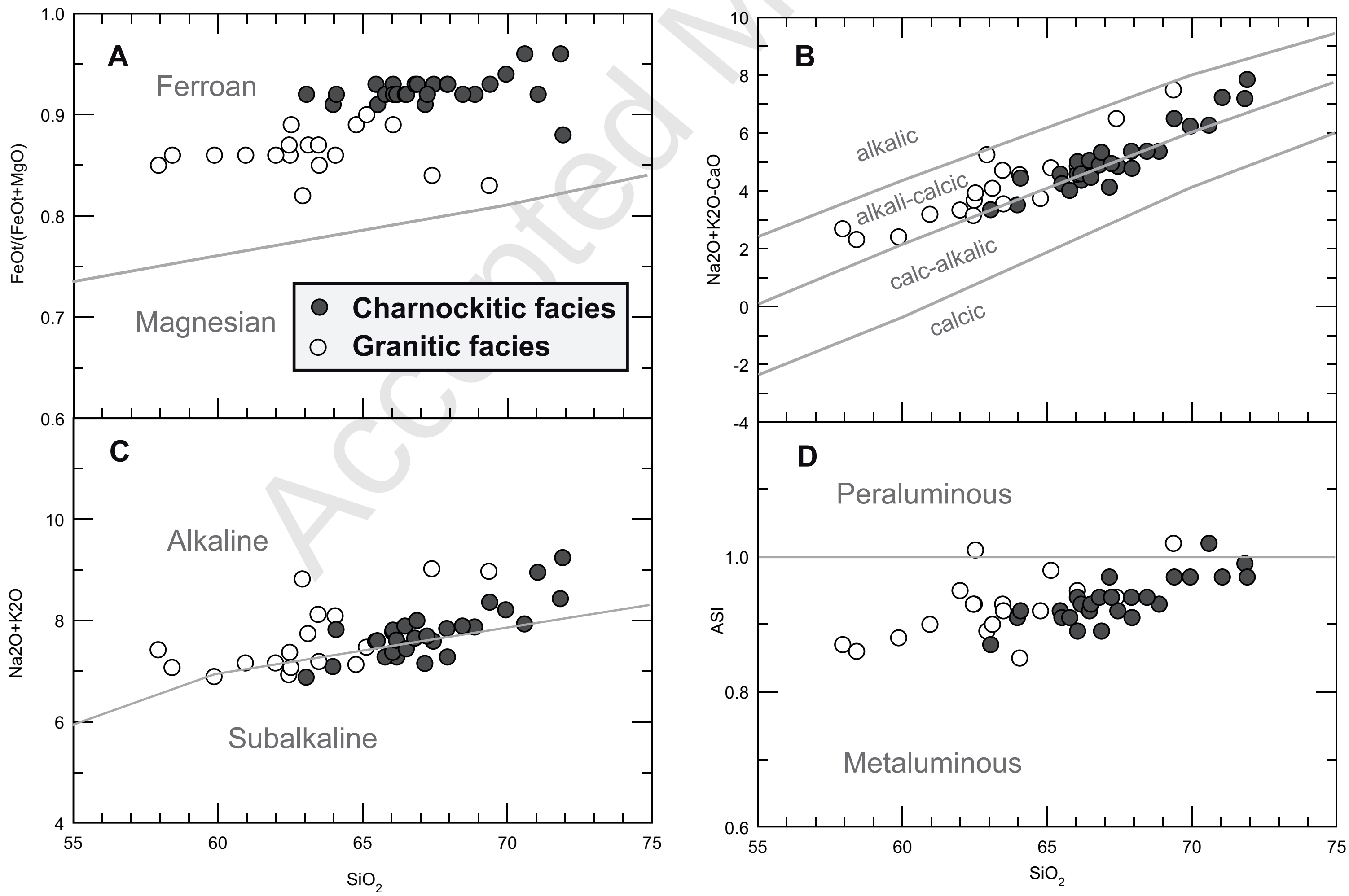

Fig. 6 - Vander Auwera et al.

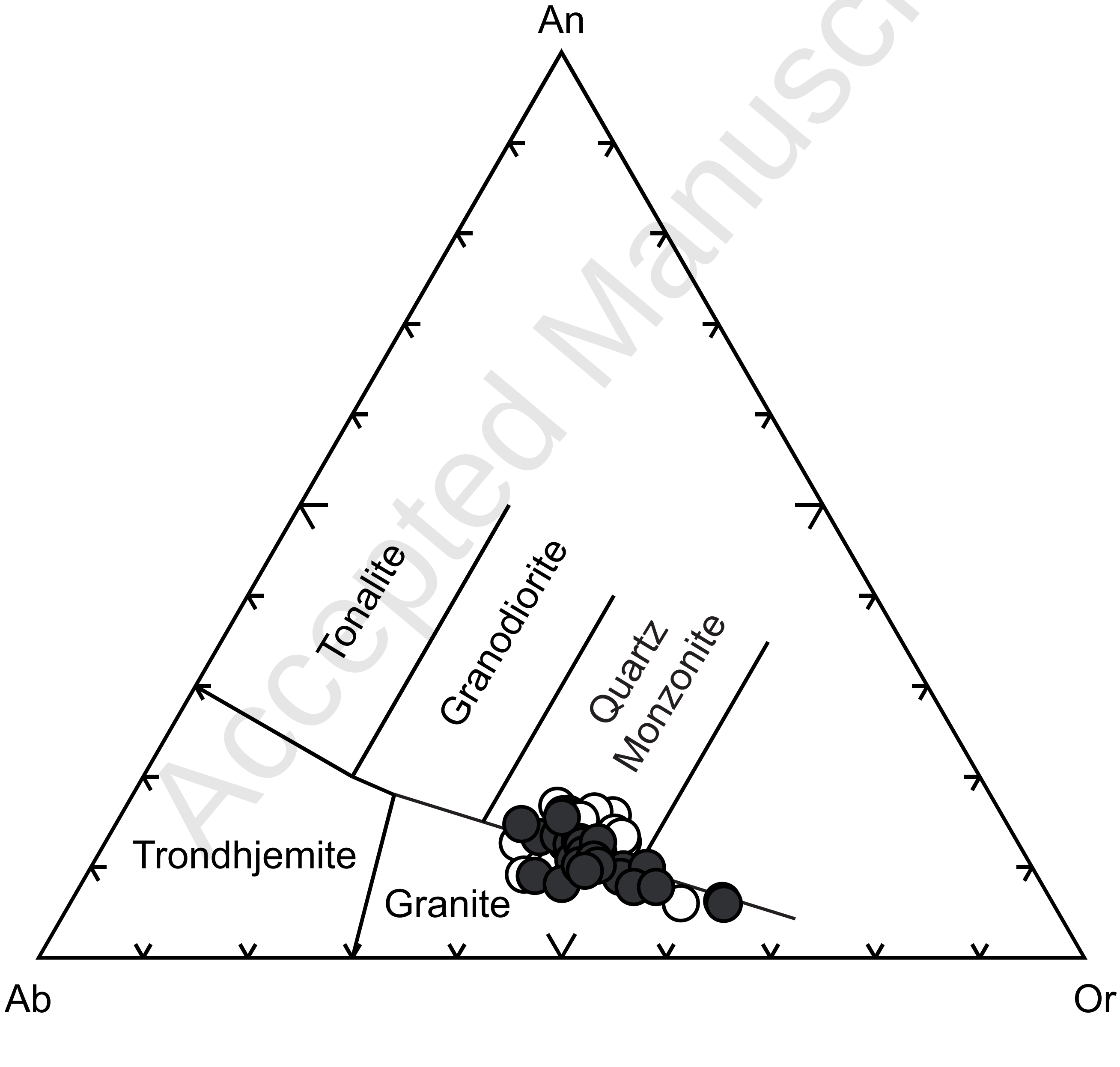

Fig. 7 - Vander Auwera et al.

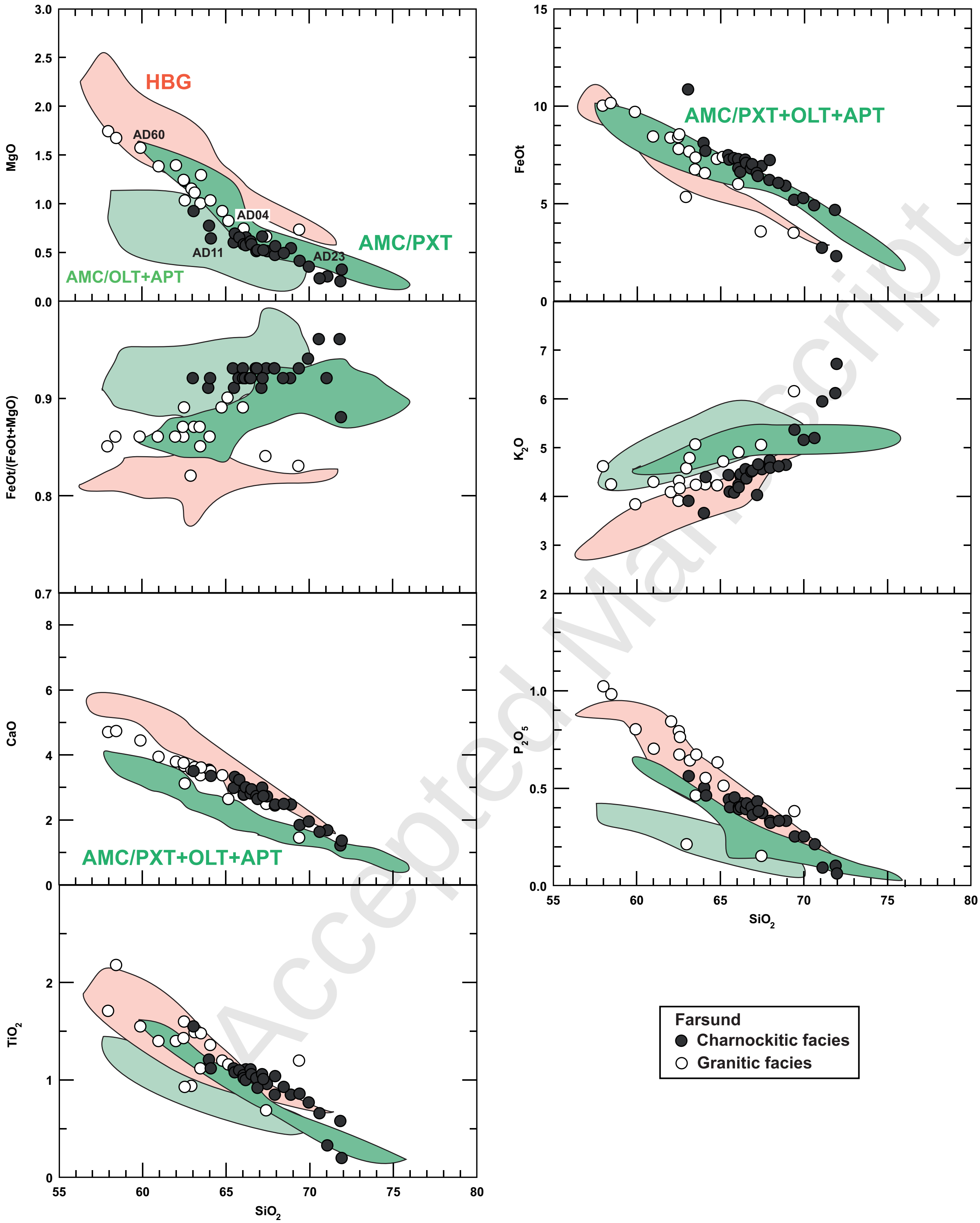

Fig. 8 - Vander Auwera et al.

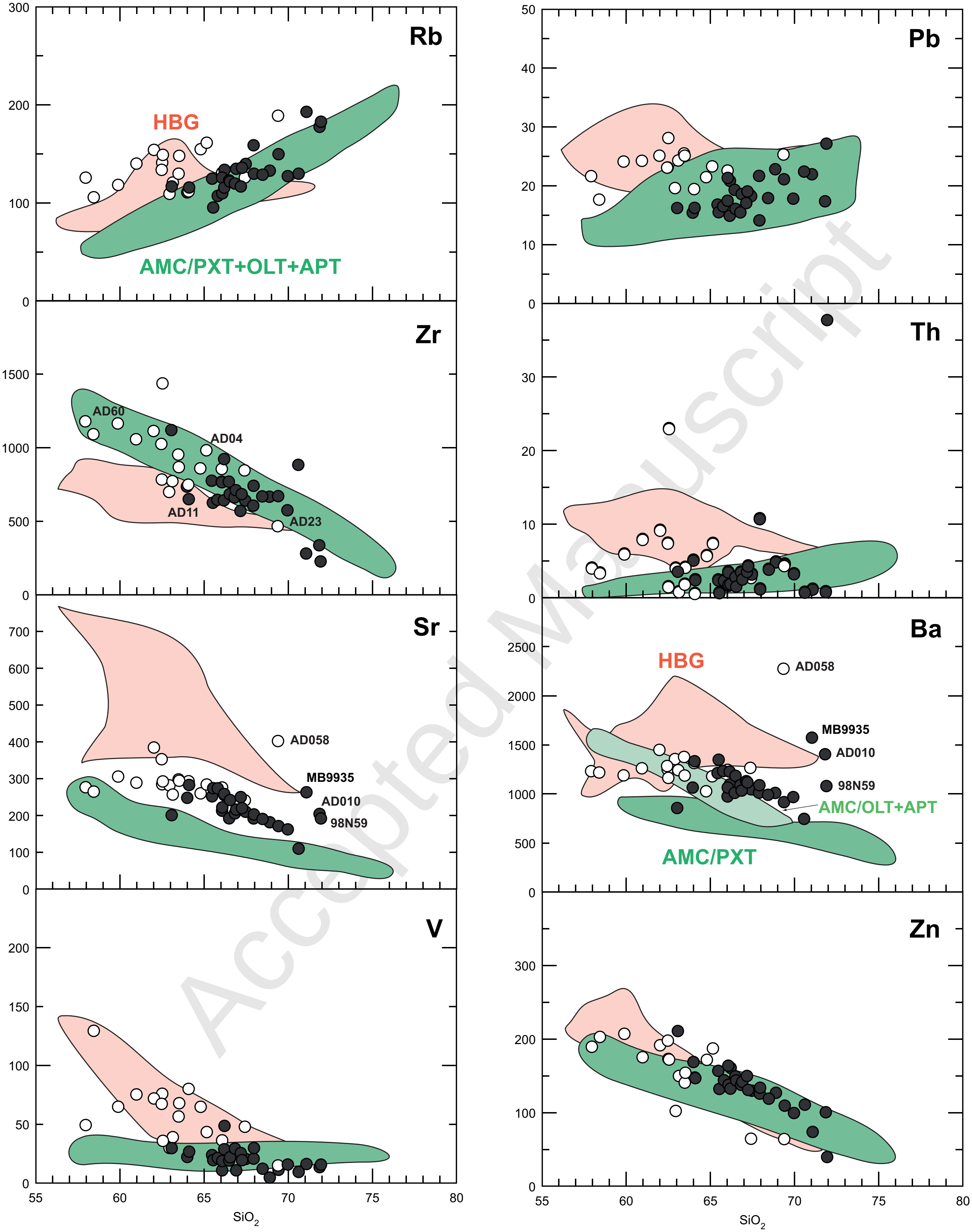

Fig. 9 - Vander Auwera et al.

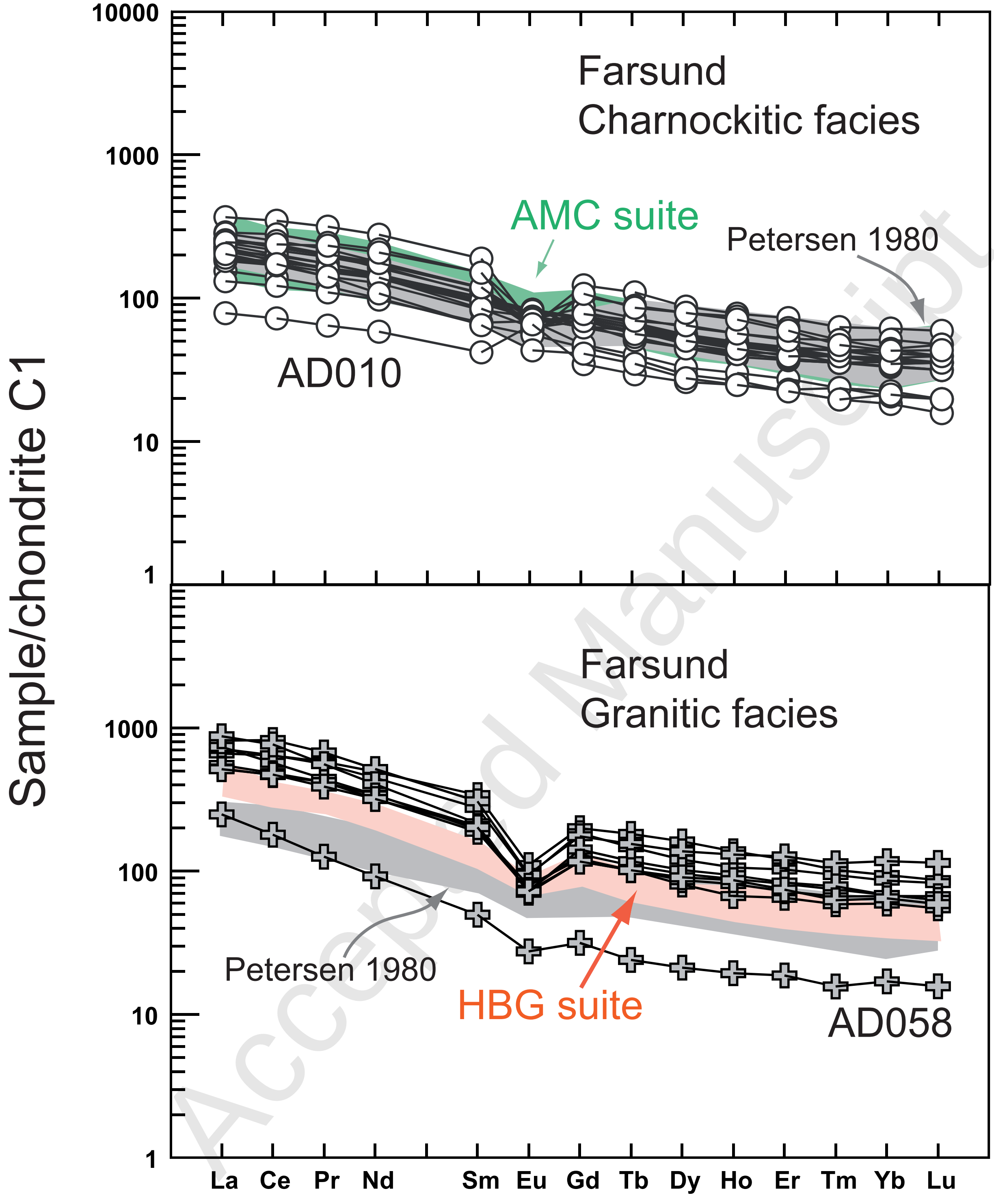

Fig. 10 - Vander Auwera et al.

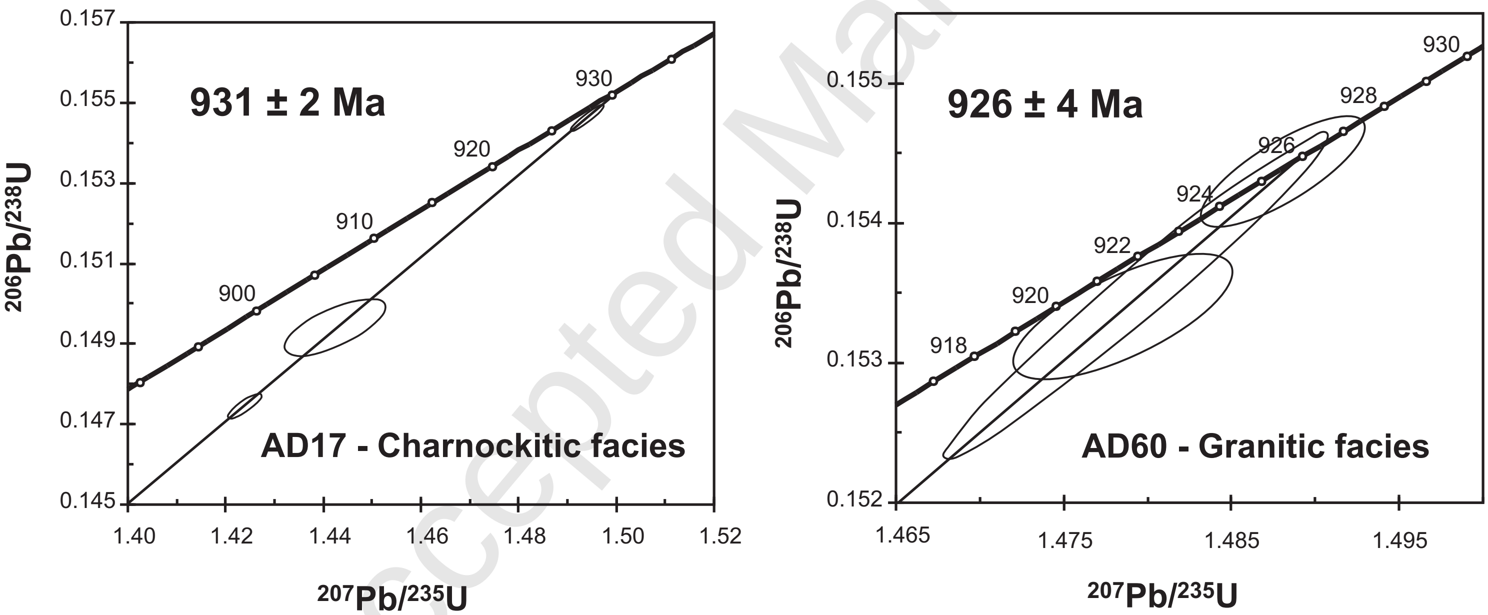

Fig. 11- Vander Auwera et al.

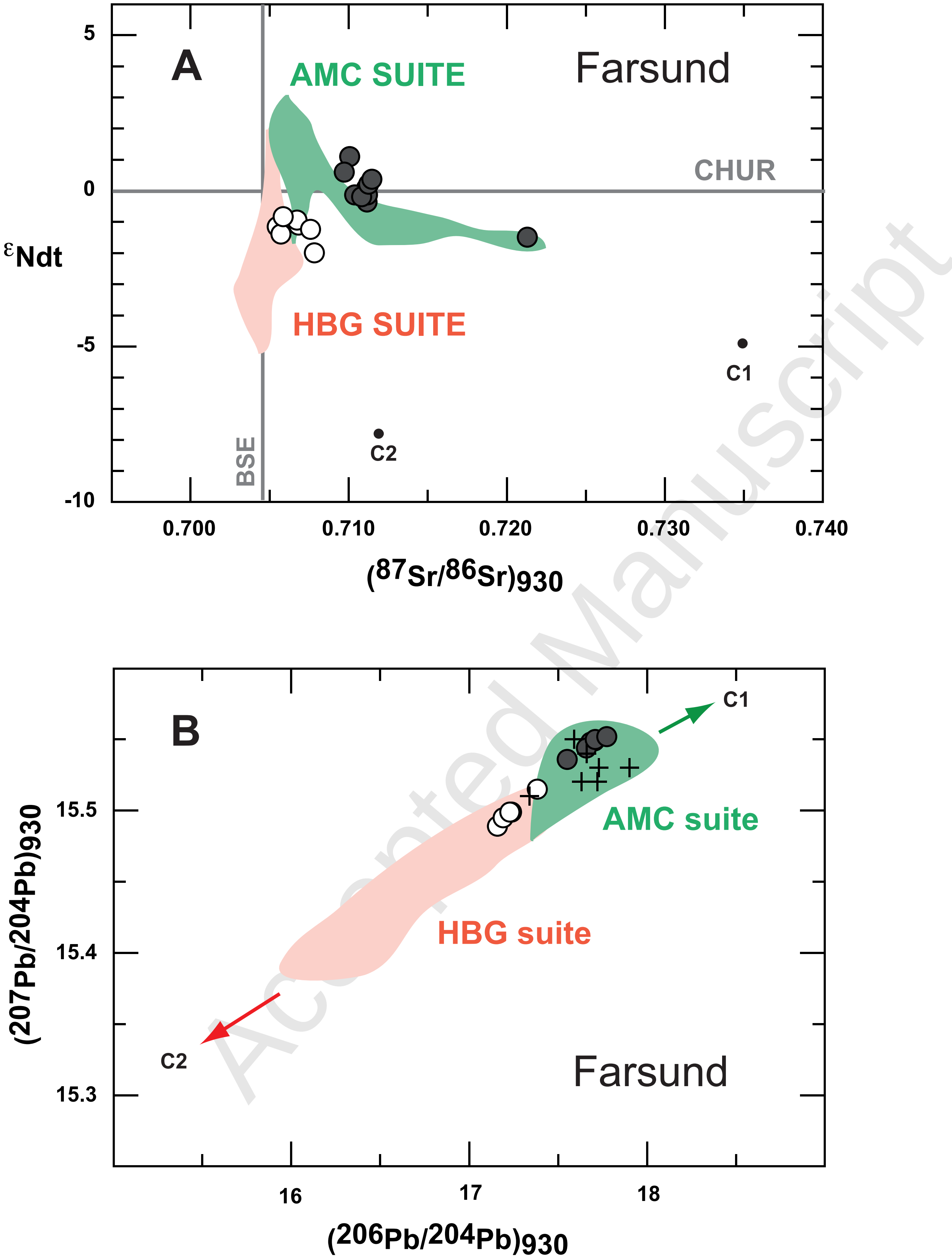

Fig. 12- Vander Auwera et al.

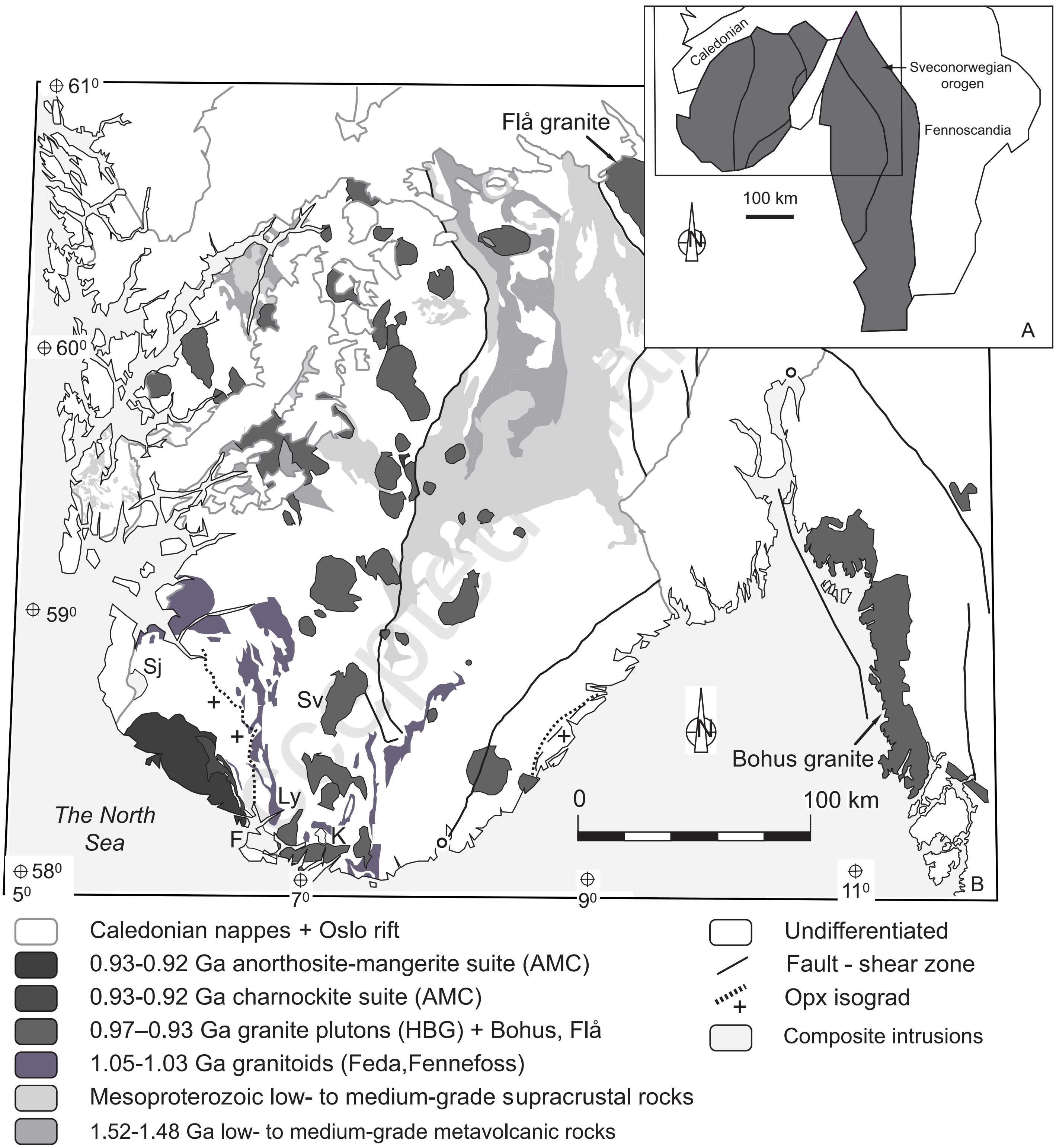

Fig. 1 - Vander Auwera et al.

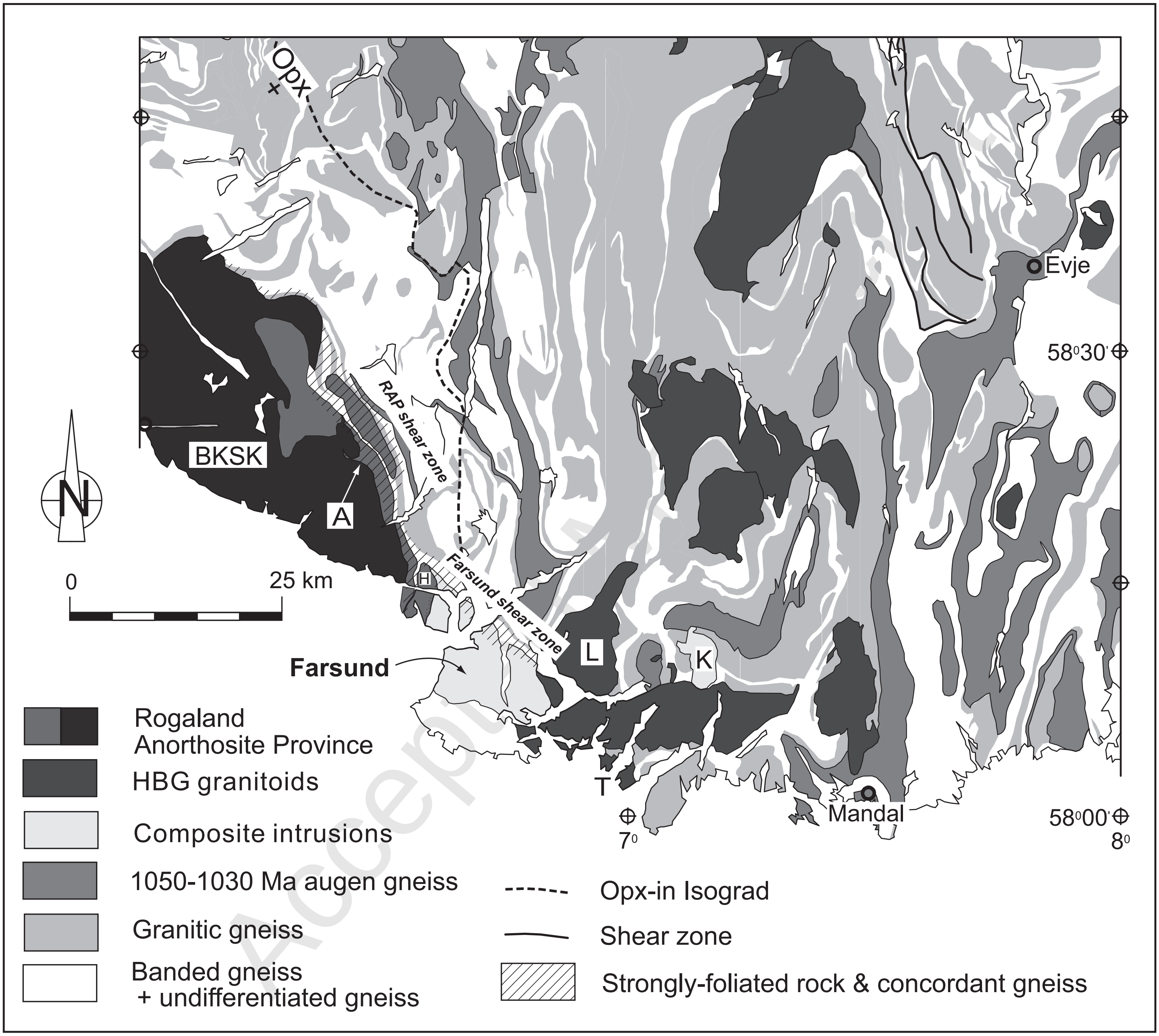

Fig. 2 - Vander Auwera et al.

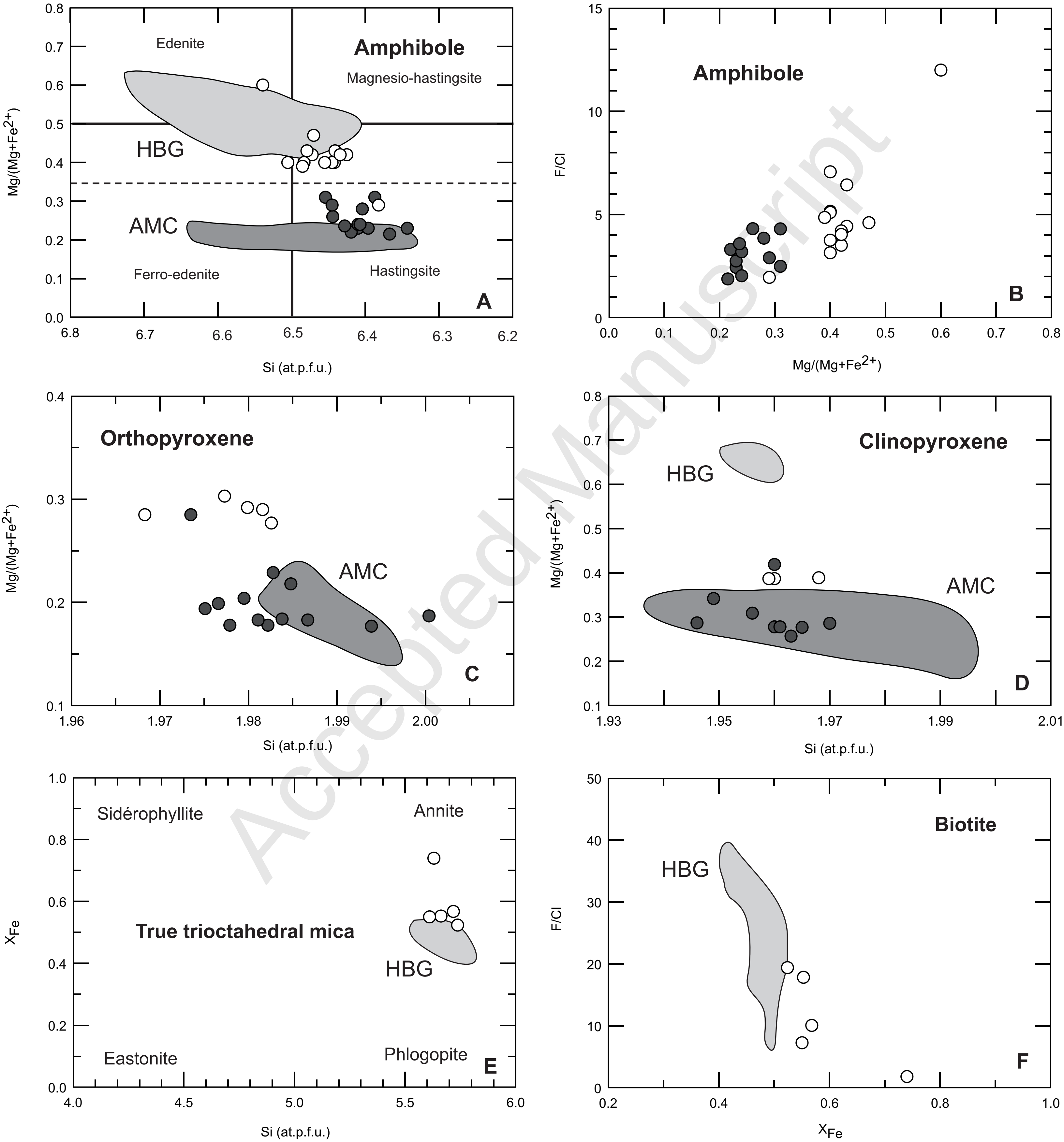

Fig. 5 - Vander Auwera et al.

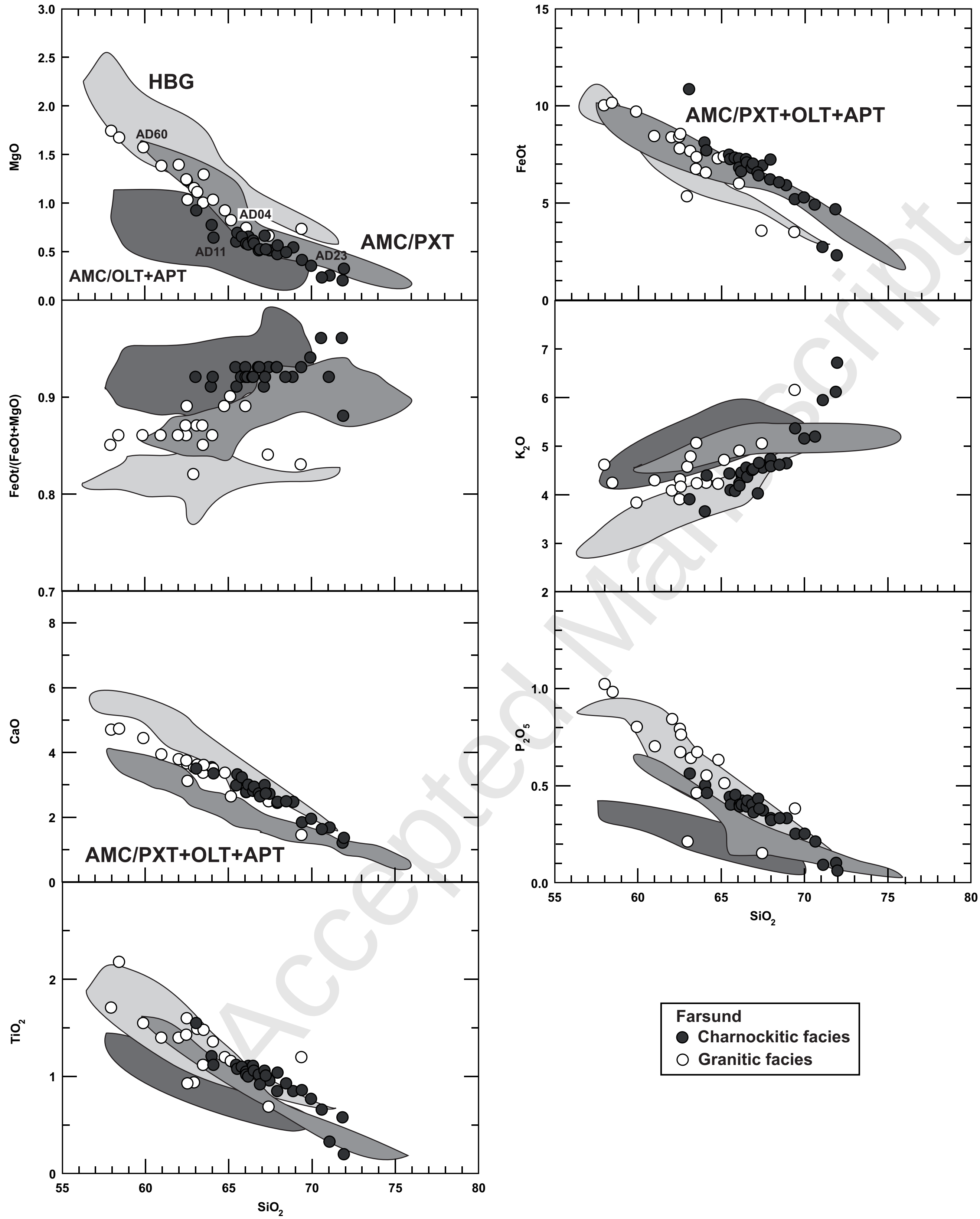

Fig. 8 - Vander Auwera et al.

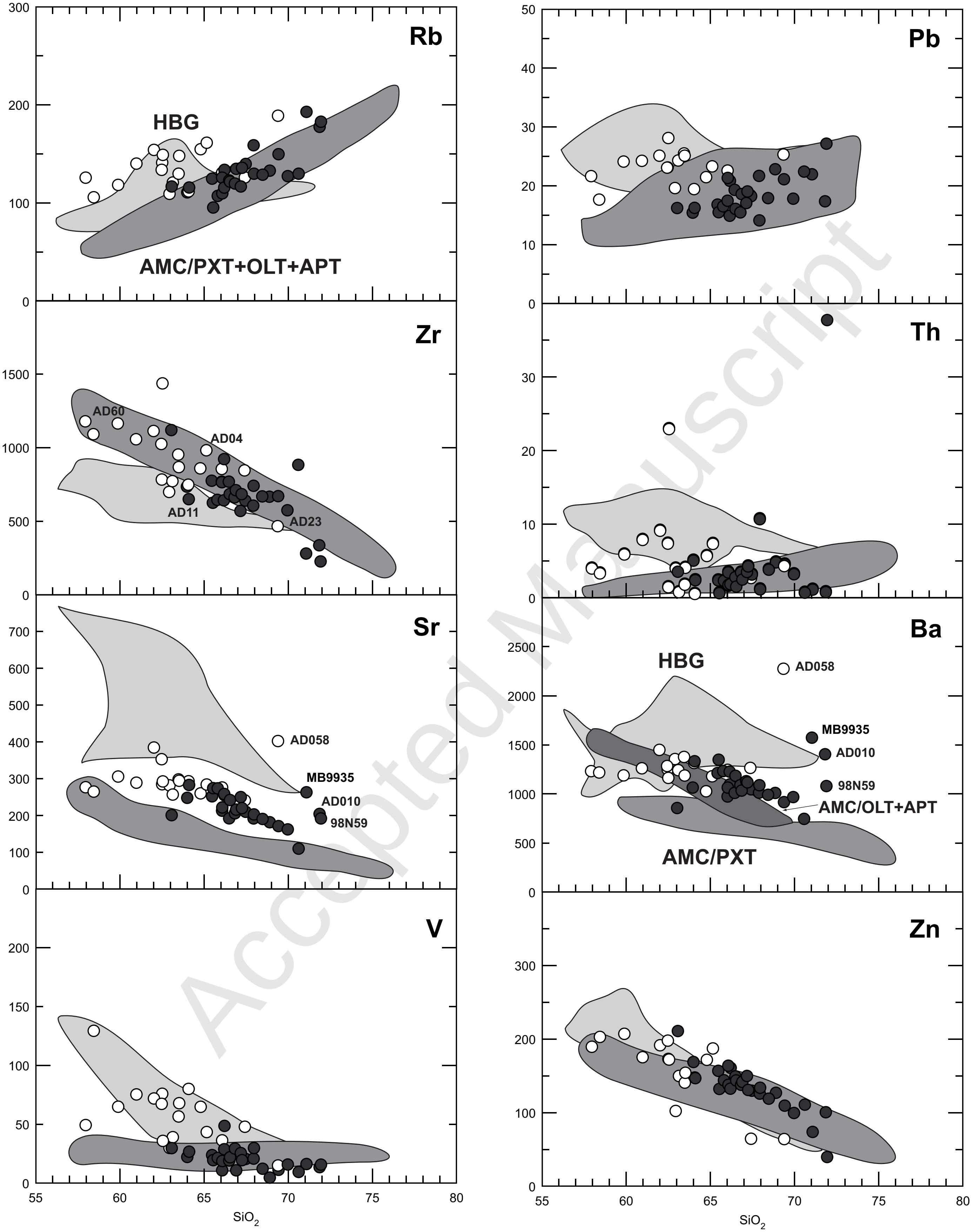

Fig. 9 - Vander Auwera et al.

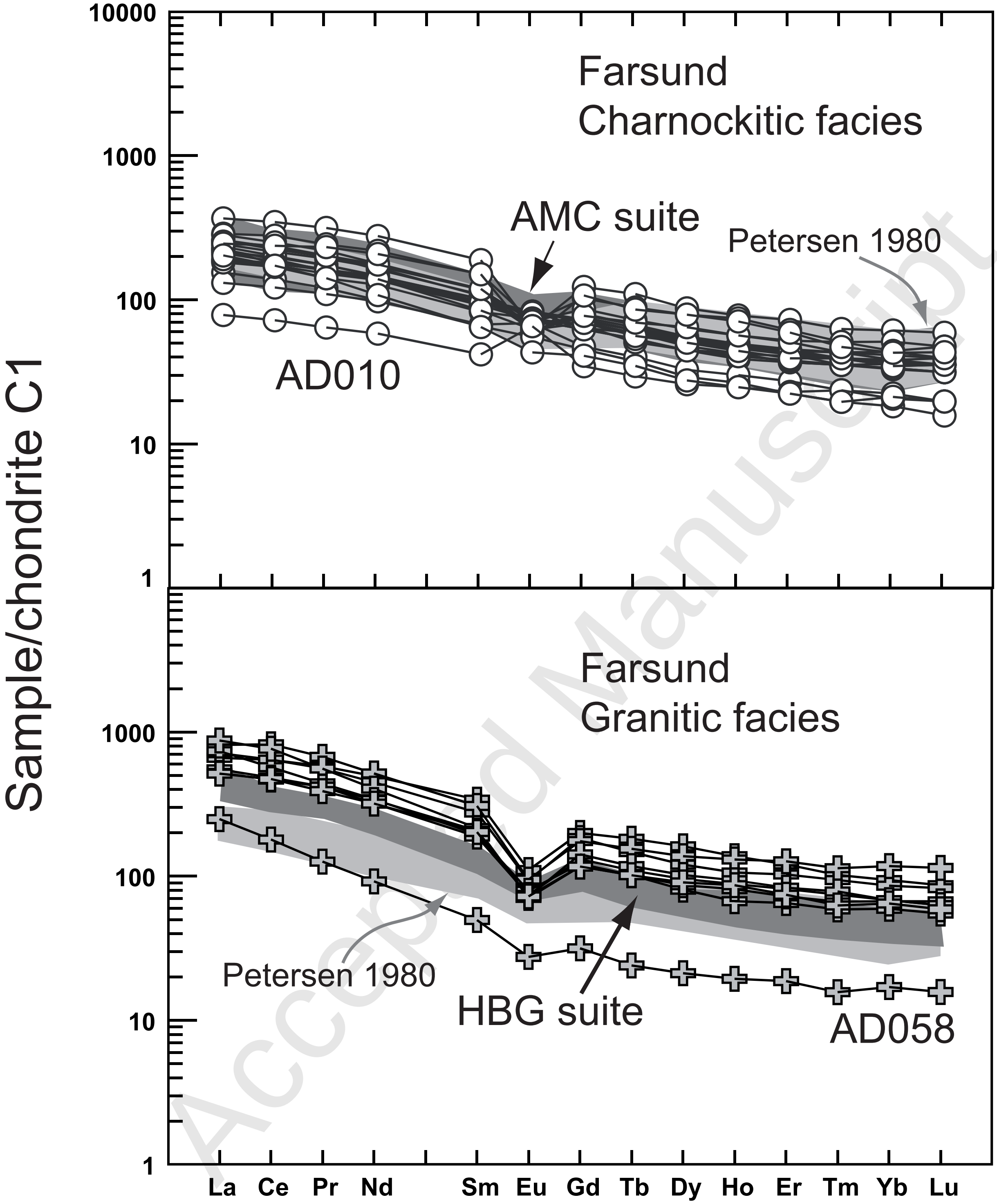

Fig. 10 - Vander Auwera et al.

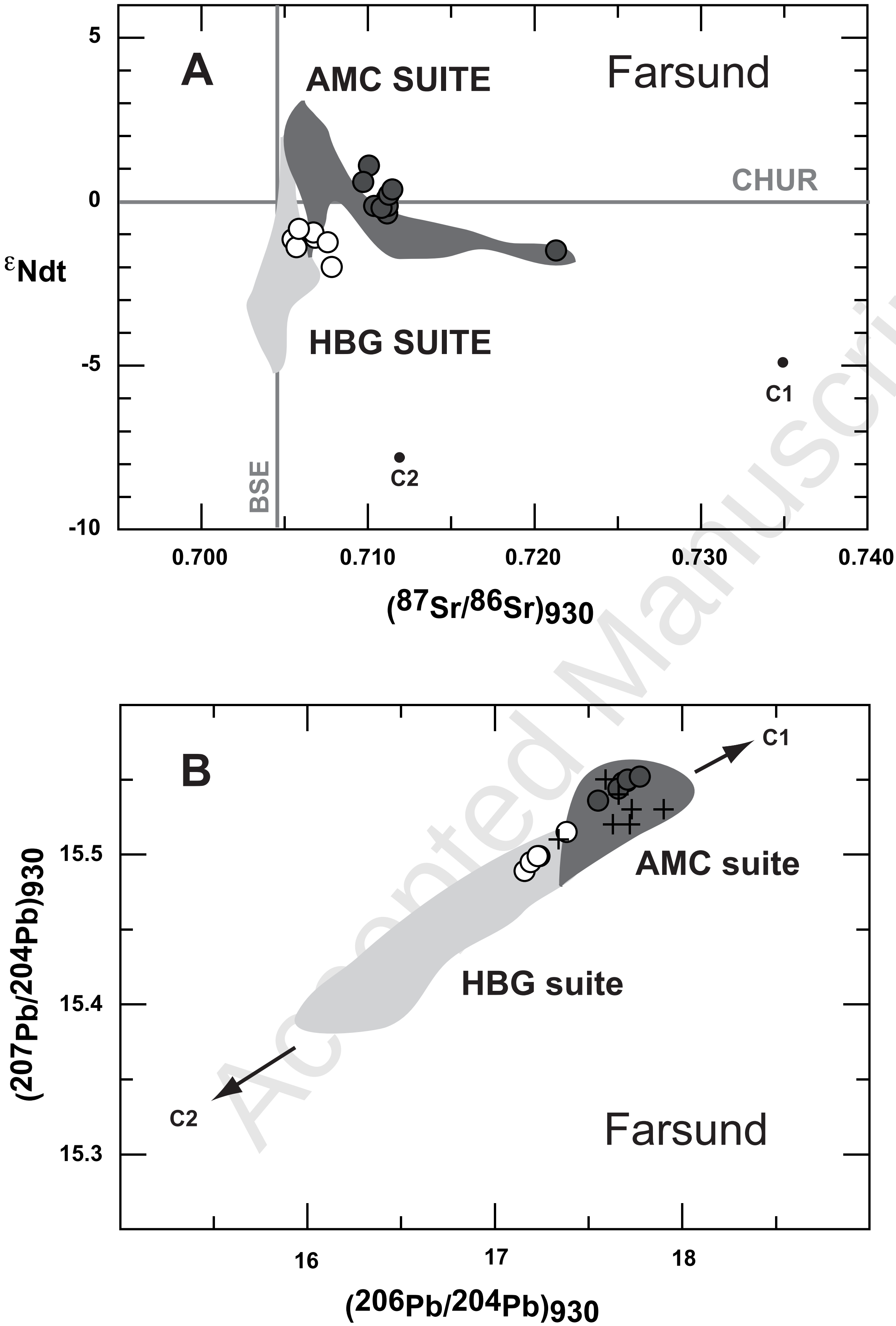

Fig. 12- Vander Auwera et al.